ADVANCED FUNCTIONAL MATERIALS

DOI: 10.1002/adfm.200500891

Theoretical Design of Catalysts for the Heterolytic Splitting of H_2**

By *Łukasz Maj* and *Wojciech Grochala**

This contribution commemorates the 240th anniversary of the discovery of elemental H_2 ('inflammable air') by Henry Cavendish in 1766

Here, we briefly review recent advances in H_2 storage technologies relying on mixed proton–hydride and destabilized hydride materials. We establish a general relationship across different materials: the higher the effective H content, the higher the temperatures needed to completely desorb H_2. Nevertheless, several systems show promising thermodynamics for H_2 desorption; however, the desorption kinetics still needs to be improved by the use of appropriate catalysts. Prompted by the importance of heterolytically splitting stable dihydrogen molecules for proton–hydride technologies, we attempt to theoretically design novel H_2 transfer catalysts. We focus mainly on $M_4Nm_4H_8$ catalysts (M = V, Ti, Zr, Hf, and Nm = Si, C, B, N), which should be able to preserve their functionality in the strongly reducing environment of a H_2 storage system. We are able to determine the energy of H_2 detachment from these molecules, as well as the associated energy barriers. In order to optimize the properties of the catalysts, we use isoelectronic atom-by-atom substitutions, vary the valence electron count, and borrow the concept of near-surface alloys from extended solids and apply it to molecular systems. We are able to obtain control over the enthalpy and electronic barriers for H_2 detachment. Molecules with the coordinatively unsaturated >Ti=Si< unit exhibit particularly favorable thermodynamics and show unusually small electronic barriers for H_2 detachment (>0.27 eV) and attachment (>0.07 eV). These and homologous ZrSi frameworks may serve as novel H_2 transfer catalysts for use with emerging lightweight hydrogen storage materials holding 5.0–10.4 wt % hydrogen, such as Li_2NH, $Li_2Mg(NH)_2$, Mg_2Si, and LiH/MgB_2 (discharged forms). Catalytic properties are also anticipated for appropriate defects on the surfaces and crystal edges of solid Ti and Zr silicides, and for Ti=Si ad-units chemisorbed on other support materials.

1. Introduction

The coupling reaction between protons and hydride anions (where both species are bound in various chemical compounds) leads to the evolution of H_2 by

$$H^+ + H^- \rightarrow H_2(g)\ (\Delta H^0 = -17.35\ \text{eV for species in the gas phase}) \quad (1)$$

This reaction typically has a large thermodynamic driving force due to i) the exothermicity of the process and ii) the increase in entropy due to the formation of a gaseous product.[1] As a consequence, the reverse reaction, i.e., the heterolytic splitting of H_2 associated with its addition to a chemical system, is usually not facile. Therefore, for the majority of promising solid hydrogen storage materials (HSMs), such as MgH_2, $NaAlH_4$, and $LiBH_4$, the charging process, until recently, has relied on the addition of H_2 to the discharged material via a two-electron redox reaction accompanied by the *homolytic* splitting of a dihydrogen molecule.[2]

Over the last four years, several important lightweight HSMs have been developed that are able to attach hydrogen via the *heterolytic* splitting of H_2. The thermal decomposition of these systems proceeds according to the following representative equations, listed here with their standard reaction enthalpy values, ΔH^0:

$$LiH + Li_2NH \rightarrow Li_3N + H_2\ (\Delta H^0 = +1.20\ \text{eV}) \quad (2)[3]$$

$$LiH + LiNH_2 \rightarrow Li_2NH + H_2\ (\Delta H^0 = +0.47\ \text{eV}) \quad (3)[3]$$

Analogous reactions for magnesium imide, MgNH,[4] and its mixtures with Li_2NH,[5] for magnesium nitride, Mg_3N_2, and its

[*] Dr. W. Grochala, Ł. Maj
Laboratory of Intermolecular Interactions
Department of Chemistry
University of Warsaw
Pasteur 1, 02093 Warsaw (Poland)
E-mail: wg22@cornell.edu
Dr. W. Grochala
Laboratory of Technology of Novel Functional Materials
Interdisciplinary Center for Mathematical and Computational Modeling
University of Warsaw
Pawińskiego 5a, 02106 Warsaw (Poland)

[**] The authors gratefully acknowledge the Interdisciplinary Center for Mathematical and Computational Modeling, ICM, and the Department of Chemistry (Warsaw, Poland) for financial support. Calculations were performed at the holk cluster of the TASK Academic Computer Center (Gdańsk, Poland); preliminary results were obtained using the ICM supercomputers. Supporting Information is available online from Wiley InterScience or from the author.

mixtures with Li_3N[6] and Li_2NH,[7] for mixtures of $LiBH_4$ and $LiNH_2$,[8] and for $LiAlH_4$ with $LiNH_2$[9] have also been studied.[10] The hydrogen-rich B–N systems constitute another important family of HSMs:

$$(NHBH)_\infty \rightarrow BN + H_2 \quad (4)^{[11]}$$

$$(NH_2BH_2)_\infty \rightarrow (NHBH)_\infty + H_2\ (\Delta H^0 = -0.25\ eV) \quad (5)^{[12]}$$

$$(NH_3BH_3) \rightarrow (NH_2BH_2)_\infty + H_2\ (\Delta H^0 = -0.22\ eV^{[12]}\ to\ -0.01\ eV\ in\ SiO_2) \quad (6)^{[13]}$$

The first observations of the release of H_2 from hydrogenated carbon nanostructures mixed with LiH according to

$$LiH + C_{nano}H \rightarrow Li + C_{nano} + H_2 \quad (7)^{[7,14]}$$

have been published in 2005.

Equation 7 somewhat resembles analogous textbook hydrolysis reactions

$$LiH + LiOH \rightarrow Li_2O + H_2\ (\Delta H^0 = -0.24\ eV) \quad (8)^{[15,16]}$$

$$1/4\ NaBH_4 + 1/2\ H_2O \rightarrow 1/4\ NaBO_2 + H_2\ (\Delta H^0 = -0.55\ eV) \quad (9)^{[15,17]}$$

that can be controlled in the solid state (Eq. 8) or in solution (Eq. 9).

In all the processes listed above, a proton–hydride coupling (Eq. 1) is formally responsible for the release of H_2.

In addition to these systems, 'destabilized hydrides' have also been recently developed, which release H_2 by

$$2\ MgH_2 + Si \rightarrow Mg_2Si + 2\ H_2\ (\Delta H^0 = +0.38\ eV) \quad (10)^{[18]}$$

$$2\ LiBH_4 + MgH_2 \rightarrow 2\ LiH + MgB_2 + 4\ H_2\ (\Delta H^0 = +0.42\ eV) \quad (11)^{[19]}$$

The initial stages of the recharging process for these important lightweight H_2 storage systems likely involve the heterolytic splitting of H_2 on the surface of Mg_2Si or MgB_2, such as by

$$Mg_2Si + H_2 \rightarrow (H^{\delta-}Mg_2)(SiH^{\delta+}) \quad (12)$$

followed by subsequent hydrogen transfer from a semimetal to a metal (from Si to Mg here), which is formally a two-electron redox reaction.

The H_2 release processes listed in Equations 2–12 are characterized by a broad range of associated standard enthalpy values, ranging from about +1.20 eV per H_2 molecule (Eq. 2) to about –0.55 eV per H_2 molecule (Eq. 9). The majority of these reactions are irreversible 'on board' (Eqs. 5, 6, 8, and 9) (i.e., they are difficult to reverse at a modest overpressure of H_2), and only a few (Eqs. 3 and 10) are relatively close to thermodynamic equilibrium under normal conditions.[20]

Łukasz Maj was born in Kielce, Poland, in 1983. He attended the Jan Kochanowski High School in Radom. As a high school student he was a laureate of the national Chemistry Olympiad and of the Annual Chemistry Competition organized by the Technical University of the city of Radom. He now studies at the Department of Chemistry, University of Warsaw, specializing in new materials. Lukasz is currently doing his M.Sc. with Dr. Wojciech Grochala, working on theoretical design of catalysts for heterolytic splitting of dihydrogen. Aside from chemistry his interest is in Asian—especialy Japanese— cinema, and in Ibero-American and Spanish literature. He is also a big fan of soccer.

Wojciech Grochala was born in Warsaw, Poland, in 1972. His education and scientific carrier are ultimately linked to the Department of Chemistry, University of Warsaw, where he received his Ph.D. and D.Sc. in spectroscopy and physical chemistry. During postdoctoral research he studied with Roald Hoffmann (Ithaca, US), and with Peter P. Edwards (Birmingham, UK). His scientific interests encompass molecular and extended systems, high-pressure and low-temperature phenomena, unprecedented high oxidation states of transition elements, electromerism, etc. Wojciech now heads the Laboratory of Technology of Novel Functional Materials, which is a joint enterprise of the Department of Chemistry and of the Interdisciplinary Center for Mathematical and Computational Modeling. The team's work is centered around novel materials, be these superconductors, materials for hydrogen storage, molecular memory carriers, or catalysts.

ADVANCED FUNCTIONAL MATERIALS

The majority of H_2 evolution reactions from proton–hydride HSMs require thermal activation and proceed with reasonable speed only at elevated temperatures; for example, the reaction depicted in Equation 2 proceeds only at temperatures above 325 °C, the reactions shown in Equations 4 and 10 above 300 °C, the reaction shown in Equation 7 above 200 °C, the one shown in Equation 3 above 150 °C, the one shown in Equation 5 above 135 °C, the reaction depicted in Equation 6 above 80–110 °C, and the one shown in Equation 8 above 50–100 °C (Table 1, Fig. 1). The entire hydrogen content stored in these materials is released at even higher temperatures. Thus, all 'reversible' endothermic reactions occur at temperatures too high (≥150 °C) to be of use "on board" for proton-exchange membrane (PEM) and alkaline fuel cell applications (60–120 °C).[1]

Upon analyzing Figure 1 and Table 1 we note that a fatal 'perverseness law' applies for two important families of H^+–H^- storage materials: *the higher the effective H content, the higher the temperature needed to desorb it completely*.[21] Mother Nature's contrariness—or wisdom—allows for several remarkable exceptions to this empirical rule, however, to our disappointment, these materials usually show even larger thermal decomposition temperature, T_{dec}, values than expected from a monotonic dependence. The kinetics of H_2 desorption is significantly inhibited in these multiphase polycrystalline systems, and the thermodynamics is usually unfavorable; thus the prospects for meeting the U.S. Department of Energy (DOE) 2015 target seem rather bleak.[22]

The dependence of T_{dec} upon the wt % of H simply reflects a progressive thermodynamic stabilization of the proton–hydride HSM, as well as the decreasing polarization of $H^{\delta-}$ and $H^{\delta+}$ as the effective H content increases. Take for example the NH_xBH_x family: the absolute values of the effective charges on the hydride anion and proton are presumably smaller for NHBH than the corresponding values for NH_4BH_4; electrostatic $H^{\delta-}$–$H^{\delta+}$ coupling is therefore more difficult for the former species, which is why it requires a higher temperature to desorb H_2. A clarifying note is needed here: since H_2 release from a H-rich compound most often occurs in consecutive steps, the least hydrogenated compound (such as NHBH) has a higher effective hydrogen content than a H-rich species (such as NH_4BH_4), although the latter has a much larger overall H content as compared to the former.

The strength of our approach, which allows the detection of the 'perverseness law', lies in the division of the decomposition reactions for various H^+–H^- storage materials into important elementary steps. This also allows us to study the specific thermodynamics and kinetics of each step. For example, Li_3N is not listed in Table 1 (or shown in Fig. 1) as a 10.3 wt % storage material ($Li_3N + 2H_2$); instead, Li_3N and Li_2NH HSMs are shown separately. Such a division is indispensable in terms of practical applications, since these materials have significantly different thermodynamics (1.20 eV vs. 0.47 eV in this case!) and very distinct thermal decomposition temperatures. It is worth remembering that other hydride HSMs, such as alanates, show a similar behavior.

Importantly, the T_{dec} values for many of the abovementioned HSMs are far from their lower thermodynamic limits (wherever data is available), leaving space for further improvement—and hope for the scientific community. For example, the lowest (theoretical) T_{dec} value is as low as +74 °C for the reaction in Equation 3 and +7 °C for the reaction depicted in Equation 10; these estimates have been obtained from the reaction enthalpies alone, neglecting the (typically unknown) specific heat capacities of the reaction substrates and products. The successful realization of the theoretical limits of the T_{dec} values for these

Table 1. Values of ΔH^0, T_{dec}, and wt % H for two families of proton–hydride HSMs: $(BN)H_x$ and $(Li,Mg)(B,N)H_x$. The charged forms of the HSMs are also listed. Species which do not follow the usual T_{dec} versus wt % H dependence (see Fig. 1), and instead show positive or negative deviations, are marked here as 'exceptions'. Four important systems which have not yet been sufficiently studied are also listed (their dehydrogenation would lead to Li_3AlN_2, MgB_2, etc.). The T_{dec} value refers to the temperature at which the entire claimed H content is released and not just the temperature where thermal decomposition begins. The theoretical H content is shown for the BN compounds.

System	H^0 [eV]	T_{dec} [°C]	wt % H	Notes
(BN) species				
$\sim BNH_2$	endo?	410 [a]	7.5	Starts at 300°C; effective 2.6–4.0% H
BH_2NH_2	–0.25	180	6.9	Starts at 135°C
BH_3NH_3	–0.22	130	6.5	Starts at 80°C
NH_4BH_4	exo	0	6.1	Starts at –40°C
(Li,Mg)(B,N)				
$LiBH_4$+ MgH_2	0.42	400 [b]	10.4	Starts at 270°C; two steps [c]; MgB_2 is formed
$Li_3(BH_4)(NH_2)_2$	exo?	350	>10	Starts at 250°C; Li_3BN_2 is formed
$LiAlH_4$+$LiNH_2$	exo?	320	8.1	Starts at 85°C
$LiH+Mg(NH_2)_2$	0.40–0.48	300 [b]	9.1	Starts at 180°C
$LiBH_4$+$2LiNH_2$	0.24	~250	7.8	Theoretically predicted value of H^0
$LiH+3/8Mg(NH_2)_2$	endo	200	7	Starts at 120°C
LiH+LiOH	–0.24	100	6.3	Starts at 50°C
$NaBH_4+2H_2O$	–0.55	25	>6	% H much below the theoretical value
Exceptions				
$LiH+Li_2NH$	1.20 [d]	425	5.4	Starts at 325°C
$LiH+C_{nano}H_x$	endo	400	7	Starts at 200°C
MgH_2+Si	0.38	300	5	Mg_2Si forms
$LiH+LiNH_2$	0.47	250 [b]	6.5	Starts at 150°C
$LiBH_4+1.3H_2O$	exo	25	7.4	% H much below the theoretical value
Not yet studied				
MgH_2+2MgNH	endo?		3.8	H content too low
$MgH_2+Mg(NH_2)_2$	endo?		4.8	H content too low
$LiAlH_4$+$2LiNH_2$	exo ?		9.5	Ideally, only Li_3AlN_2 would be formed
$Mg(BH_4)_2$	endo?		14.9	Ideally, only MgB_2 would be formed

[a] This experimental value is for the ca. 4 wt % H system; it is likely to be smaller for stoichiometric BNH_2. [b] Catalyzed. [c] Possibly the enigmatic LiB^IH_2 form is involved. [d] This value is based on the H^0_f value of 197 kJ mol^{-1} for Li_3N (http://www.knovel.com, accessed June 2006). An even larger value is obtained using a H^0_f value of 164.56 kJ mol^{-1} (National Institute of Standards and Technology (NIST) Chemistry WebBook).

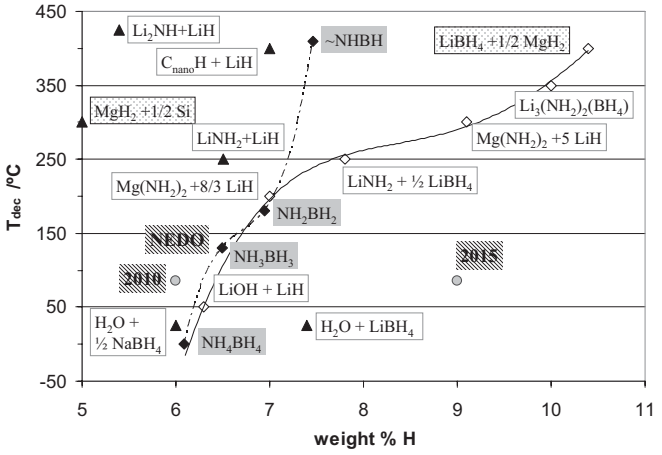

Figure 1. T_{dec} for several important proton–hydride hydrogen storage systems along with their wt % hydrogen content (data from Table 1). The T_{dec} value refers to the temperature at which the entire claimed H content is released, and not just the temperature where thermal decomposition begins. Note that all proton–hydride systems with a $T_{dec} < 150\,°C$ produce H_2 in an exothermic reaction, and are irreversible on-board. The lines have been introduced as a guide to the eye for the two different families of proton–hydride HSMs that fulfil the 'perverseness law' (filled and empty squares). Exceptions to this rule are marked with filled triangles. The New Energy and Industrial Technology Development Organization (NEDO), Department of Energy (DOE) 2010, and DOE 2015 targets are indicated.

and similar reactions can hopefully be achieved by the use of appropriate catalysts.[23] The main goal of this paper is to design such catalysts from first principles.

The heterolytic activation of H_2 (formally requiring an immense energy of 17.35 eV to produce unbound H^+ and H^-) is more difficult than homolytic activation (to produce $2\,H^\bullet$, 4.50 eV) but not impossible. Indeed, it may be achieved if the resulting proton and hydride anion form sufficiently strong chemical bonds to other elements in the reaction products. This happens for many second period p-block elements, but there are also a wide variety of transition-metal-based synthetic molecules known to be capable of heterolytically activating H_2 under quite mild conditions. Some recently developed systems include phosphine complexes of Ru,[24] Ni,[25] Pd, and Pt,[24] nitrosyl derivatives of Re,[26] mononuclear Ir species,[27] Rh–S[28] and Ti–S compounds,[29] Ir_2–S,[30] Rh_2–S,[31] binuclear RuW–S,[32] NiFe–S,[33] and many polynuclear cluster complexes,[34] to mention just a few. The applicability of these smart molecules for H_2 transfer reactions with discharged highly efficient solid HSMs has not yet been tested, but it is quite clear that they have some serious disadvantages, which will almost certainly render them unusable in automobiles on a large scale. These disadvantages include: a) they typically work only within a proper solvent, b) they contain precious transition metals, such as Ir, Ru, Pd, Ru, and Re, c) they have a large molar mass, thus substantially decreasing the efficiency of H_2 storage in a HSM–catalyst system, d) some of the catalysts include organic ligands that contain unsaturated C=C bonds; such compounds are unlikely to survive the strongly reducing environment within hydrogen storage systems, and e) they contain carefully crafted ligand environments for the transition metal, which are likely to be destroyed in the ultra-basic environment within hydrogen storage systems (for example, in a mixture of LiH and $LiNH_2$).

In this work, we target molecular catalysts built from cheap elemental constituents {(Ti, V, Zr, Hf)/(Si, C, B, N)/H}; these catalysts evolve from i) our earlier concepts of electronegativity perturbed Ti-substituted hydrocarbons,[35] ii) the landmark report on the catalytic activity of Ti compounds in the homolytic splitting of H_2,[36] and iii) from a recent theoretical contribution on the control of catalytic processes on the surfaces of subsurface alloys.[37] Catalysts studied in the present work have been designed to preserve their integrity and functionality in the aggressive chemical environment of solid proton–hydride hydrogen-storage systems.

2. Results and Discussion

2.1. Controlling the Enthalpy of the H_2 Detachment Reaction Using $Ti_4C_4H_8$-Like Species

A H_2 transfer catalyst should of course exhibit a less positive enthalpy of H_2 detachment, ΔE_{det}, than the HSM with which it will cooperate; however, an energy close to +0.40 eV per H_2 molecule is required to account for entropy effects.[38] Thus, let us first learn how to establish that a catalyst will indeed exhibit appropriate thermodynamics of H_2 attachment/detachment.

2.1.1. Controlling the ΔE_{det} Value by Isoelectronic Substitutions

Prospective catalysts described in this section are analogous to the C_8H_8 (cubane) molecule and have a formula $M_4Nm_4H_8$, where M = Ti, Zr, or Hf, and Nm = C or Si (Fig. 2A). Conceptually, these molecules can be obtained from the previously studied $Ti_4C_4H_8$[34] by isoelectronic chemical substitutions (where the valence electron count is preserved). We demonstrate the use of such substitutions as a tool to directly influence the value of ΔE_{det} in the reaction

$$M_4Nm_4H_8 \rightarrow M_4Nm_4H_6 + H_2\ (\Delta E_{det}) \qquad (13)$$

where one H comes from a tetravalent metal site, M, while another comes from a nonmetal site, Nm. A chemist will naturally expect that substitution in the sequence Ti → Zr → Hf will lead to an increased stability of the M–H bonds, and as a consequence, to more positive values of ΔE_{det}. Similarly, the C → Si substitution should lead to a decrease in ΔE_{det}. Let us examine what the density functional theory (DFT) calculations predict. The computed values of ΔE_{det} for these substitutions are shown in Table 2 (see Supporting Information for further details).

It turns out that the calculated ΔE_{det} values are entirely consistent with our qualitative predictions. The value of ΔE_{det} can be engineered over a broad energy range (+0.35 to +1.35 eV) via simple isoelectronic substitutions. Of the six computed values, two (0.35 eV for $Ti_4Si_4H_8$ and 0.40 eV for $Zr_4Si_4H_8$) fall

ADVANCED FUNCTIONAL MATERIALS

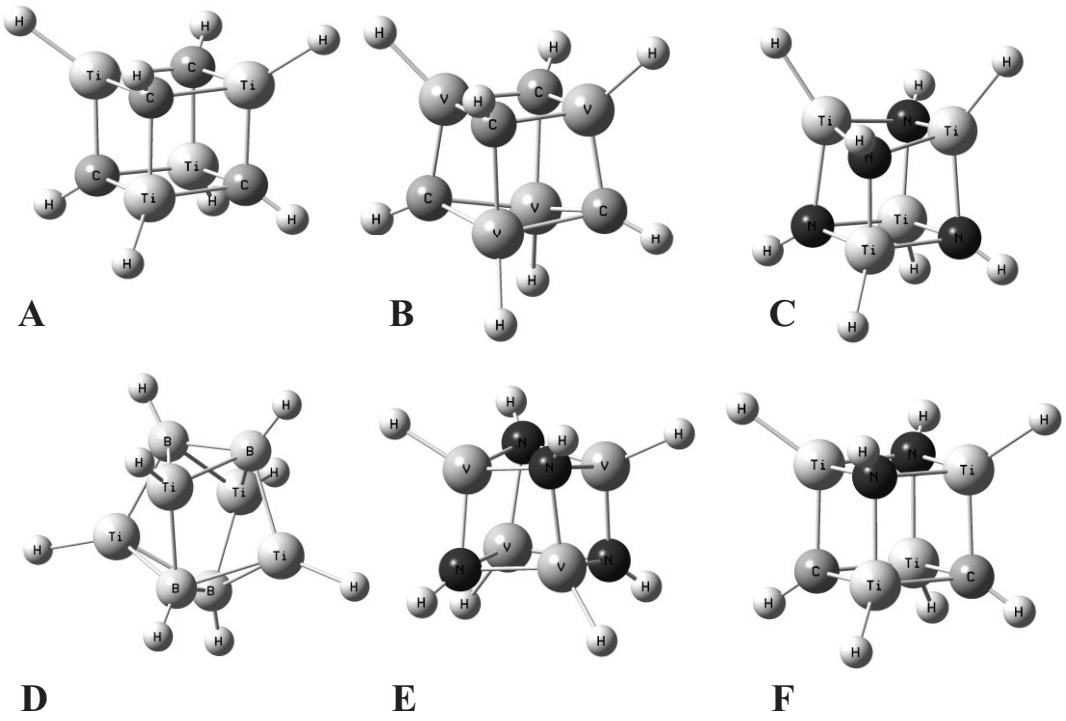

Figure 2. Six examples of molecules studied in this work: A) $Ti_4C_4H_8$; B) $V_4C_4H_8$; C) $Ti_4N_4H_8$; D) $Ti_4B_4H_8$; E) $V_4N_4H_8$; F) $Ti_4(C_2N_2)H_8$. The molecules B–F can be obtained from A by deliberate atom-by-atom substitutions; F is a molecular analogue of a near-surface alloy. Note that the geometry of the heavy element $(MNm)_4$ framework resembles a slightly distorted cube, except for D, where B–B bonds are formed.

Table 2. Zero-point energy (ZPE)-corrected values of the H_2 detachment energy for cubane-like $M_4Nm_4H_8$ molecules, where M = Ti, Zr, Hf and Nm = C, Si; the B3LYP results are presented here.

M	Nm	
	C	Si
Ti	0.91	0.35
Zr	1.06	0.40
Hf	1.35	0.68

very close to the desired narrow window (from +0.404 eV, entropy factor, (T·S(H_2)) of H_2(g) at 25 °C, to +0.505 eV, TS of H_2(g) at 100 °C). Further substitutions beyond the isoelectronic set studied here are needed to vary ΔE_{det} in a more continuous manner.[39]

2.1.2. Controlling the ΔE_{det} Value by Changes in the Valence Electron Count

Let us again utilize $Ti_4C_4H_8$ as the starting system for the following perturbations, Ti → V, and C → B, N, which affect the electron count. It is worth recalling that $Ti_4C_4H_8$ can be regarded as a polynuclear Ti(IV) compound with bridging CH^{3-} ligand groups, i.e., as $\{(H^-)Ti^{IV}(CH^{3-})\}_4$. This molecule has a significantly large computed relaxed ionization potential (8.47 eV) and a relatively small computed value for the electron affinity (2.10 eV). These values are quite similar to those for an atom of 'noble' gold (9.22 and 2.3 eV, respectively). This feature suggests that the catalyst is likely to maintain its integrity upon insertion into an aggressive proton–hydride hydrogen storage system.

Several important quasi-localized molecular orbitals (MOs) can be distinguished in the electronic structure of $Ti_4C_4H_8$:[34] i) the HOMO – 2 (highest occupied molecular orbital) at –0.2621 au, which is a bonding combination of 2p orbitals of C and d orbitals of Ti; ii) HOMO – 1 at –0.2620 au, which is another bonding combination of 2p orbitals of C and d orbitals of Ti; iii) the HOMO at –0.2619 au, which is a σ bonding combination of 1s orbitals of H^-_{Ti} and $d(z^2)$ orbitals of Ti; iv) the lowest unoccupied molecular orbital (LUMO) at –0.1265 au, which is a σ* antibonding combination of $d(z^2)$ orbitals of Ti and 1s orbitals of H^-_{Ti}, with some contribution from the 1s orbitals of H_C (the lowest unoccupied molecular orbital (LUMO) is weakly bonding between Ti atoms); v) LUMO + 1 at –0.1201 au, which is essentially a nonbonding combination of $d(x^2–y^2)$ orbitals of Ti; and vi) LUMO + 2 at –0.1200 au, which is another nonbonding combination involving the d orbitals of Ti. Selected MOs are illustrated in Figure 3.

The donor function of the molecule (HOMO) is mainly hydride-centered, while the acceptor function (LUMO) is predominantly on Ti. The Ti–H bonds are rather weak, long, and quite ionic (as compared to the Ti–C and C–H bonds), and form the uppermost σ and the lowest σ* levels of the molecule.

The MO picture should allow us to predict the consequences of varying the valence electron count (Ti → V or C → N, +1 e^- per atom; C → B, –1 e^- per atom). These variations should most

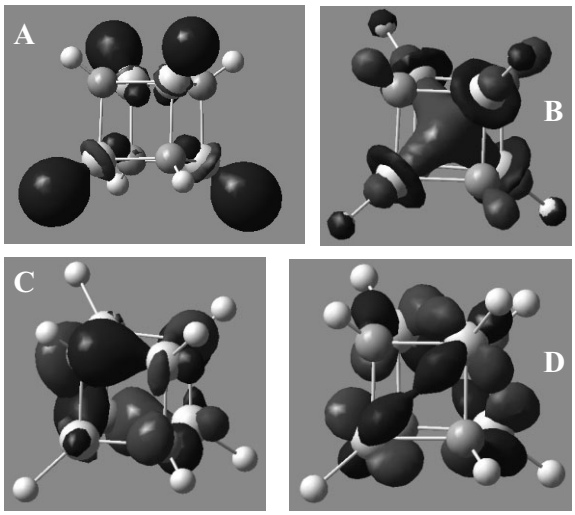

Figure 3. Kohn–Sham molecular orbitals for $Ti_4C_4H_8$: A) HOMO, B) LUMO, C) HOMO – 2, and D) LUMO + 1.

significantly influence the frontier orbitals (with a change of $\pm 2\,e^-$ per molecule), as well as the HOMO – 1 (with a change of $-4\,e^-$ per molecule) and LUMO + 1 (with a change of $+4\,e^-$ per molecule), whereas the Ti–C core (HOMO – 2, LUMO + 2) should be relatively unaffected by these variations. For example, upon the addition of two electrons per molecule, the M–H bonds should weaken and elongate (reflecting the population of a Ti–H antibonding orbital); the same result is expected upon reducing the number of electrons by two (depopulation of a Ti–H bonding orbital). Consequently, the energy of H_2 detachment should decrease in both cases, as one H is eliminated from the Ti site. Upon the addition of an additional two electrons to the system (which corresponds to a complete Ti → V or C → N substitution), the nonbonding LUMO + 2 orbital is occupied, and this is unlikely to lead to further changes in ΔE_{det}. Upon withdrawal of a total of four electrons from $Ti_4C_4H_8$, the resulting depopulation of HOMO – 1 should invoke an increase in the M–Nm separation, and so on.

A similar analysis can be done for other kinds of chemical substitutions; unfortunately, HOMO – 2, HOMO – 1, and HOMO are virtually degenerate on the energy scale, and the LUMO, LUMO + 1, and LUMO + 2 show a similar behavior. This means that variations in the valence electron count will induce strong vibronic coupling in the system, which will influence all quasi-degenerate MOs and thus all important chemical bonds. The exact predictions will therefore rely on explicit calculations for all the chemical species in question.

The effect of the Ti → V and C → B, N substitutions in the $Ti_4C_4H_8$ molecule upon the calculated energy of H_2 detachment (Figs. 2B–E and Supporting Information) is summarized in Table 3.

To our surprise, the calculated changes of the ΔE_{det} value for substituted analogues of $Ti_4C_4H_8$ often show good agreement with the simplistic MO-based predictions, despite the substantial quasi-degeneration of MOs in the vicinity of the HOMO and LUMO. For example, a decrease or increase in the number

Table 3. ZPE-corrected values of the H_2 detachment energy (eV) for $M_4Nm_4H_8$ molecules, where M = Ti, V, and Nm = B, C, N; the DFT Becke 3-Parameter Lee, Yang and Parr (B3LYP) results are presented here.

M	Nm			
	B	C	N	B N
Ti	0.40 [a]	0.91	0.42 [a]	0.07 [b], 1.26 [c]
V	0.54 [a]	0.54 [a]	0.46 [a]	not determined

[a] Molecule with various non-equivalent M–H and Nm–H bonds; we list the value of ΔE_{det} associated with the dehydrogenation path leading to the most thermodynamically stable product. [b] H_2 detachment from Ti and N. [c] H_2 detachment from Ti and B.

of valence electrons by four (yielding $Ti_4B_4H_8$, $Ti_4N_4H_8$, $V_4C_4H_8$) always leads to decreased stability of the molecule with respect to heterolytic H_2 elimination (as compared to the $Ti_4C_4H_8$ standard). The ΔE_{det} values are comparable regardless of the nature of atomic substitutions (0.40 eV for $Ti_4B_4H_8$, 0.42 eV for $Ti_4N_4H_8$, 0.54 eV for $V_4C_4H_8$). However, the trends expected for other properties are poorly reproduced. For example, the average Ti–H distances in $Ti_4N_4H_8$ (1.770 Å) (Fig. 2C) are indeed slightly longer than for $Ti_4C_4H_8$ (1.746 Å), but those for $Ti_4B_4H_8$ (Fig. 2D) are somewhat shorter (1.738 Å). Similarly, the V–H bond lengths computed for $V_4C_4H_8$ (1.685 Å) (Fig. 2B) are shorter than the Ti–H distances in $Ti_4C_4H_8$ (1.746 Å), which does not agree with the predictions (see Supporting Information for numerical data).[40]

Two interesting co-substitutions can be performed that leave the overall electron count unchanged: one is $C_4 \rightarrow B_2N_2$, while another is a simultaneous Ti → V and C → B exchange. The first perturbation leads to $Ti_4(B_2N_2)H_8$; this species shows some resemblance to the parent $Ti_4C_4H_8$ in terms of geometry: the Ti–H distances (1.742–1.745 Å) are similar to those in $Ti_4C_4H_8$ (1.746 Å), while the average of the B–H (1.234 Å) and N–H (1.024 Å) bond lengths is 1.129 Å, which is similar to the C–H bond length in $Ti_4C_4H_8$ (1.102 Å). The average of the Ti–B (2.097 Å) and Ti–N (2.027 Å) distances is 2.062 Å, which is again very close to the average Ti–C distance (2.037 Å).[41]

H_2 can be detached from $Ti_4(B_2N_2)H_8$ in at least two different ways, either from Ti and N, or from Ti and B. The corresponding energies of H_2 detachment differ quite substantially: 0.07 eV for detachment from Ti and N, and 1.26 eV for detachment from Ti and B (compared to 0.91 eV for Ti and C in $Ti_4C_4H_8$). Thus, the isoelectronic $C \rightarrow (B_{1/2}N_{1/2})$ substitution seems to greatly affect the energetics and decomposition path of $Ti_4Nm_4H_8$.[42] The total number of valence electrons turns out not to be the major determinant of the H_2 detachment energy.

Notably, the simultaneous Ti → V and C → B substitution (which also does not change the overall electron count) significantly influences both the molecular geometry (the bonding pattern changes substantially) as well as the ΔE_{det} value (ΔE_{det} decreases from +1.02 eV for the Ti–C compound to +0.70 eV for the V–B analogue), which is quite different from the behavior expected using a simple MO approach. The quasi-degeneracy of MOs in the vicinity of the HOMO and LUMO is to be blamed for these shortcomings.

ADVANCED FUNCTIONAL MATERIALS

Intuitively, one is tempted to discard these poorly performing systems and focus on the best candidates. With a ΔE_{det} value close to +0.40 eV,[20] $Ti_4B_4H_8$ naturally becomes the molecule of choice for subsequent studies on the impact of chemical substitutions on the ΔE_{det} value. One may anticipate that substituting Ti → Zr → Hf in the $Ti_4B_4H_8$ molecule will lead to a small increase in the corresponding ΔE_{det} values, similar to the behavior seen for $Ti_4Nm_4H_8$ (Nm = C, Si) derivatives (as described in Section 2.1.1). However, this is not exactly the case. The computed ΔE_{det} values are 0.40, 0.38, and 0.69 eV for the Ti, Zr, and Hf derivatives, respectively, thus suggesting that $Zr_4B_4H_8$ may be as important as the parent Ti-based system.

To summarize this section, $Ti_4Si_4H_8$ (0.35 eV), $Zr_4B_4H_8$ (0.38 eV), $Zr_4Si_4H_8$ (0.40 eV), $Ti_4N_4H_8$ (0.42 eV), $Ti_4B_4H_8$ (0.44 eV), and $V_4N_4H_8$ (0.46 eV) have been identified as the most promising catalytic candidates, considering only the thermodynamics of the heterolytic addition of H_2.

2.2. Controlling the Kinetics of H_2 Attachment/Detachment

In the second step of the catalyst design process, let us learn to control the kinetic aspects of H_2 attachment/detachment. This is certainly a more difficult task than controlling the overall reaction thermodynamics, but will guide us to genuine catalyst candidates. However, first it is worth revisiting the relationship between the kinetics and thermodynamics of the H_2 detachment reaction for a broad range of stoichiometric binary hydrides of main group and transition metals.

2.2.1. 'Golden Rule' for Stoichiometric Binary Hydrides: 'Thermodynamics Controls Kinetics'

The experimentally observed dependence of the 'effective energy barrier' for homolytic H_2 detachment, $\Delta E^{\#}_{effective}$, upon a thermodynamic reaction parameter (standard redox potential for the metal cation/metal pair in aqueous solution, E^0), for a wide range of inorganic binary hydrides, is shown in Figure 4. Here, $\Delta E^{\#}_{effective}$ (in eV) has been calculated from experimental T_{dec} values (in K) for the hydrides as

$$\Delta E^{\#}_{effective} = 3/2 k T_{dec}/(1.602 \times 10^{-19}) \quad (14)$$

where the dominator represents the conversion factor from joules to electron volts. Numerical data (see Section S10 of Supporting Information) for this plot has been taken from Grochala et al.[1]

$\Delta E^{\#}_{effective}$ is meant to reproduce only a fraction of the true energy barrier for the H_2 detachment reaction, $\Delta E^{\#}_{det}$, which rises on the potential energy surface of the reaction. For a system where the energy partitioning function is controlled by a Maxwell–Boltzmann distribution, at a given temperature T, only a small number of the molecules have sufficient energy for the decomposition reaction to proceed towards thermodynamic equilibrium. Since $\Delta E^{\#}_{effective}$ is associated with the average energy of particles, it must be about an order of magnitude smaller than, but still proportional to, $\Delta E^{\#}_{det}$.

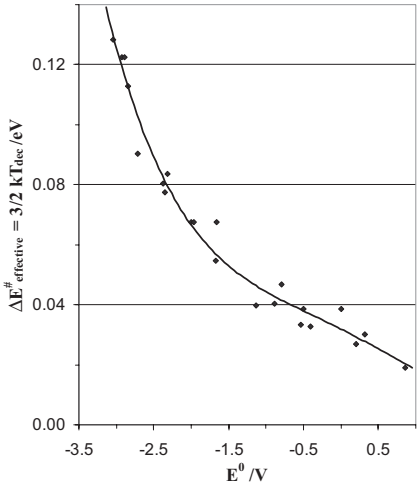

Figure 4. Experimentally observed dependence between the 'effective energy barrier' for homolytic H_2 detachment, $\Delta E^{\#}_{effective}$ (in eV), and a thermodynamic reaction parameter (standard redox potential for the metal cation/metal pair in aqueous solution, E^0 (in V)), for a broad range of inorganic binary hydrides of metallic and semimetallic elements. See text and Supporting Information for details.

As seen in Figure 4, $\Delta E^{\#}_{effective}$ shows a nice variation with the value of E^0 (a thermodynamic parameter), according to the scenario: the larger the thermodynamic stability of the hydride, the larger is the effective barrier for H_2 detachment.[43] A similar 'golden rule', usually called Hammond's rule in the literature,[44] is also frequently encountered for many other types of chemical reactions, as well as for catalytic reactions occurring on crystal surfaces. Unfortunately, as is known from experiments, reaching the thermodynamic equilibrium requires too large of an energy barrier for many lightweight binary and ternary metal hydrides; their decomposition at practicable speeds usually requires temperatures of ca. 200 °C, and catalysts are necessary to facilitate operation at lower temperatures. A similar behavior is seen for proton–hydride storage materials.

As we will show in the next few sections, it may be possible, using two of the molecules studied in this contribution, to achieve a very low energy barrier for heterolytic H_2 detachment, while still preserving the thermodynamics of the reaction at close to neutral under standard conditions.

2.2.2. Reaction Pathways for the Detachment of H_2 from $M_4Nm_4H_8$ Species

The process of H_2 detachment from the $M_4Nm_4H_8$ species (M = Ti, Zr; Nm = B, C, N, Si) is associated with a TS and two concomitant energy barriers: $\Delta E^{\#}_{det}$ and $\Delta E^{\#}_{att}$ (Fig. 5). $\Delta E^{\#}_{det}$ increases when the reaction progresses from $Ti_4Nm_4H_8$ via a dihydrogen complex (H_2C) as

$$M_4Nm_4H_8\ (substrate) \rightarrow M_4Nm_4H_6 \cdots H_2\ (H_2C) \quad (15)$$

whereas $\Delta E^{\#}_{att}$ is related to the reverse reaction.

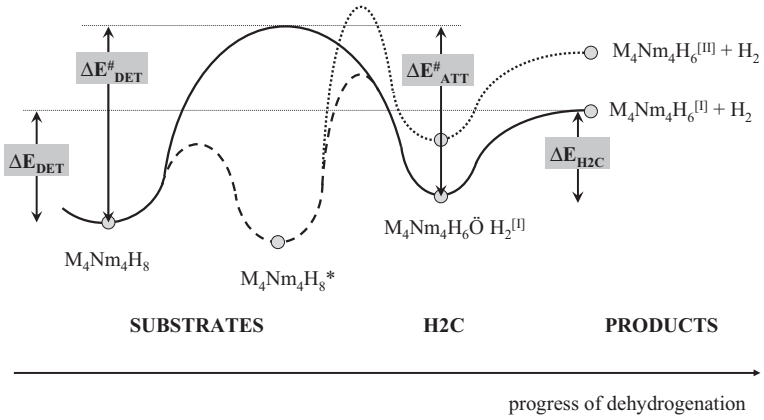

Figure 5. A generalized reaction path for H_2 detachment from $M_4Nm_4H_8$ molecules. A cubane-like $M_4Nm_4H_8$ molecule can be dehydrogenated to the most stable product ($M_4Nm_4H_6^{[II]}$) in a two-step reaction (solid line) involving the most stable dihydrogen complex intermediate ($M_4Nm_4H_6\cdots H_2^{[I]}$). The set of thermodynamic parameters (ΔE_{det}, $\Delta E^{\#}_{det}$, $\Delta E^{\#}_{att}$, ΔE_{H_2C}) associated with this reaction are marked by arrows. For some systems, a low-energy $M_4Nm_4H_8$* isomer also exists, which has a terminal M–H bond and a bridging Nm···H···M bond. This dehydrogenation path (dashed line) shows two smaller barriers instead of a large one. For some molecules, the second most thermodynamically stable product ($M_4Nm_4H_6^{[II]}$) may be formed upon dehydrogenation (dotted line). The label for $M_4Nm_4H_6\cdots H_2^{[II]}$ and the path leading directly from $M_4Nm_4H_8$ to $M_4Nm_4H_6^{[II]}$ have been omitted for brevity.

The dihydrogen complex with the H_2 molecule weakly attached to an acidic M site can be further decomposed to the final gaseous products

$$M_4Nm_4H_6\cdots H_2\ (H_2C) \rightarrow M_4Nm_4H_6 + H_2(g) \quad (16)$$

Our calculations indicate that H_2C is formed spontaneously from $Ti_4Nm_4H_6$ and H_2 (as long as no entropy term is considered) and there is no electronic barrier to this elemental process. The stability of H_2C is thus determined only by the size of the gain in reaction energy relative to the inhibiting entropy factor, with the barrier to this reaction being purely an entropic one.

Obviously, the following relationship holds,

$$\Delta E_{det} = \Delta E^{\#}_{det} - \Delta E^{\#}_{att} - \Delta E_{H_2C} \quad (17)$$

where ΔE_{H_2C} is the (always negative) energy of formation of the dihydrogen complex from $M_4Nm_4H_6$ and $H_2(g)$ (Fig. 5). The values of $\Delta E^{\#}_{det}$ and $\Delta E^{\#}_{att}$ are very important in the context of the catalytic action: if $\Delta E^{\#}_{att}$ is small, then H_2 absorption by the catalyst will be fast; if in addition $\Delta E^{\#}_{det}$ is also small, then the barrier for H_2 transfer to the discharged HSM is also likely to be small.

The molecules studied here show a variety of different chemical bonding arrangements and cover a broad range of molecular properties. Not surprisingly, the substrates ($M_4Nm_4H_8$), reaction intermediates ($M_4Nm_4H_6\cdots H_2$), and reaction products ($M_4Nm_4H_6$) may in some cases exhibit several isomers. For example, while scrutinizing the potential energy surfaces of $M_4Nm_4H_8$ molecules (M = Ti, Zr and Nm = Si, or M = Ti and Nm = B), we have detected local minima for structures other than the cubane-like geometries studied in Sections 2.1.1 and 2.1.2 (see Supporting Information for details). These important isomers of the reaction substrates, denoted hereafter by an asterisk (*) alongside their molecular formula, contain bridging M···H···Nm three-center bonds and thus represent interstitial hydrides. In some cases they are more stable than the cubane-like species (such as for M = Ti, Zr and Nm = Si), while in others they have a comparable energy (as for M = Ti and Nm = B). Therefore, the reactions shown in Equations 15 and 16 may proceed from $M_4Nm_4H_8$, first via $M_4Nm_4H_8$*, and then via H_2C, to the final products,

$$M_4Nm_4H_8 \rightarrow M_4Nm_4H_8^* \rightarrow M_4Nm_4H_6\cdots H_2 \rightarrow M_4Nm_4H_6 + H_2(g) \quad (18)$$

as calculated for M = Ti, Nm = Si (Section 2.3.1).

On the other hand, the obtained reaction products (i.e., $M_4Nm_4H_6$ molecules and their corresponding H_2C complexes) may also have several isomers which differ in energy and other properties from the most stable minimum. Here, we consider only reactions proceeding to the most stable isomer of $M_4Nm_4H_6$ that we could find (such reactions are denoted by a superscripted [I] accompanying the molecular formula, whereas the second most stable isomer is denoted by [II]). Naturally, the resulting values of ΔE_{det}, $\Delta E^{\#}_{det}$, and $\Delta E^{\#}_{att}$ will vary for each separate set of isomers of reactants and products involved in the reactions depicted in Equations 15–18 (Fig. 5).

In the next section we proceed to analyze the calculated values of the reaction enthalpies and reaction barriers for several Ti- and Zr-containing systems discussed above.

2.2.3. Barriers for H_2 Detachment from $M_4Nm_4H_8$ Species

Table 4 summarizes the values of ΔE_{det}, ΔE_{H_2C}, $\Delta E^{\#}_{det}$, and $\Delta E^{\#}_{att}$ for nine molecules with rather complex potential energy surfaces. For each of these molecules we have been able to detect the transition state (TS) for the H_2 detachment reaction. In addition, data are shown for three molecular analogues of subsurface alloys; these will be discussed in detail in Section 2.2.5. The {ΔE_{det}, $\Delta E^{\#}_{det}$} and {ΔE_{det}, $\Delta E^{\#}_{att}$} values for all the studied compounds are collectively plotted in Figure 6, along with the ΔE_{det} values for several reversible hydride–proton HSMs, and the limiting $T{\cdot}S(H_2)$ term at three different temperatures, where $S(H_2)$ is the entropy of gaseous H_2.

It turns out that the calculated barrier for the H_2 detachment reaction, $\Delta E^{\#}_{det}$, is rather large for a majority of the $M_4Nm_4H_8$ catalyst candidates, and quite surprisingly, is quite independent of the value of ΔE_{det} for reactions leading to the most thermodynamically stable isomer of the $M_4Nm_4H_6$ product. This is exemplified by the $\Delta E^{\#}_{det}$ values for $Ti_4C_4H_8$, $Ti_4N_4H_8^{[I]}$, $Ti_4B_4H_8^{[I]}$, and $Zr_4B_4H_8^{[I]}$, which exceed 0.8 eV, and the corresponding $\Delta E^{\#}_{att}$ values, which are greater than 0.65 eV (except for $Ti_4C_4H_8$). At the same time, ΔE_{det} varies over a wide range in these systems, from an optimal value of 0.38 eV to the exces-

ADVANCED FUNCTIONAL MATERIALS

Table 4. ZPE-corrected values of the H_2 detachment energy (ΔE_{det}) and barrier for H_2 detachment ($\Delta E^{\#}_{det}$) for selected $(M,M')_4(Nm,Nm')_4H_8$ molecules, and of the barrier for H_2 attachment to corresponding $(M,M')_4(Nm,Nm')_4H_6$ molecules ($\Delta E^{\#}_{att}$), where M, M′ = Ti, V, Zr and Nm, Nm′ = B, C, N, Si. The energy for dihydrogen complex formation (ΔE_{H_2C}) from H_2 and $(M,M')_4(Nm,Nm')_4H_6$, as well as the H···H separation ($R(H\cdots H)_{TS}$) in the TS during the dehydrogenation reaction, are also shown here. These are DFT/B3LYP results; see Supporting Information for further details. [I] denotes the most thermodynamically stable $(H^-)M\cdots Nm(H^+)$ product of the reaction depicted in Equations 15 and 16. [II] denotes the second most thermodynamically stable product of the reaction shown in Equations 15 and 16.

M/Nm	ΔE_{det} [eV]	$\Delta E^{\#}_{det}$ [eV]	$\Delta E^{\#}_{att}$ [eV]	ΔE_{H_2C} [eV]	$R(H...H)_{TS}$ [Å]	Comments
$Ti_4(N_2C_2)H_8$	+0.99	1.16	0.40	–0.22 [a]	2.206	[b]
$Ti_4C_4H_8$	+0.91	1.07	0.30	–0.13	1.047	[b]
$(V_2Ti_2)C_4H_8$*	+0.79	0.80	0.15	–0.14	1.036	[c]
$Ti_4(B_2C_2)H_8$*	+0.69	1.07	0.53	–0.14	1.027	[c]
$Ti_4N_4H_8^{[II]}$	+0.64	1.06	0.49	–0.07 [a]	1.058	[b]
$Ti_4B_4H_8^{[II]}$	+0.55	0.85	0.40	–0.10 [a]	1.081	[d]
$Zr_4Si_4H_8$*	+0.54	0.47	0.07	–0.13	1.088	[e]
$Zr_4B_4H_8^{[II]}$	+0.53	N.D.[f]	N.D.[f]	–0.03 [a]	N.D.	[b]
$Ti_4Si_4H_8$*	+0.49	0.31	0.00	–0.18	1.046	[e]
$Ti_4N_4H_8^{[I]}$	+0.42	1.28	1.20	–0.34	1.064	[b]
$Ti_4B_4H_8^{[I]}$	+0.40	0.97	0.68	–0.11	1.178	[b]
$Zr_4B_4H_8^{[I]}$	+0.38	1.47	1.14	–0.05	1.551	[b]

[a] H_2C breaks the C_s symmetry. [b] The 'interstitial' minimum* (four terminal NmH bonds, three terminal MH bonds, and one bridging Nm···H···M bond) is not stable. [c] Cubane-like minimum (four terminal NmH and four terminal MH bonds) is not stable. [d] Cubane-like minimum is –0.03 eV below minimum* with a bridging Nm···H···M bond. [e] Cubane-like minimum is +0.14 eV above minimum* with a bridging Nm···H···M bond. [f] Complex reaction path; no TS has been detected.

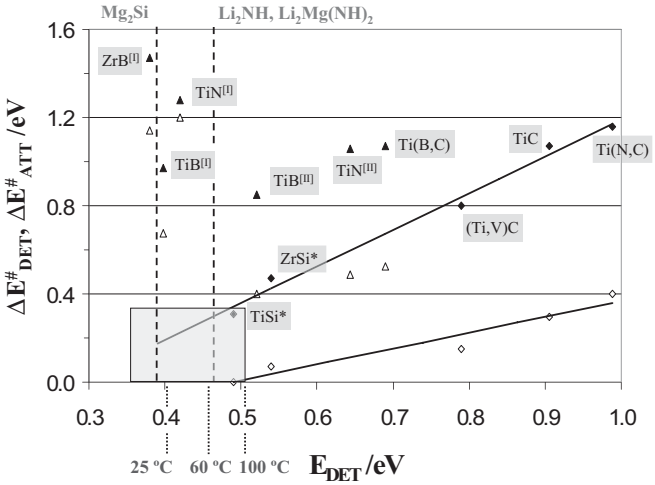

Figure 6. Plot of the ZPE-corrected values for $\{\Delta E_{det}; \Delta E^{\#}_{det}\}$ (filled symbols) and $\{\Delta E_{det}; \Delta E^{\#}_{att}\}$ (open symbols) for selected molecular catalyst candidates studied in this work. ΔE_{det} is the H_2 detachment energy, $\Delta E^{\#}_{det}$ is the barrier to H_2 detachment for selected $(M,M')_4(Nm,Nm')_4H_8$ molecules, while $\Delta E^{\#}_{att}$ is the barrier for H_2 attachment to corresponding $(M,M')_4(Nm,Nm')_4H_6$ molecules, where M, M′ = Ti, V, Zr and Nm, Nm′ = B, C, N, Si. The heavy constituent elements of a molecule are shown for each entry. The enthalpy values for H_2 detachment from three important HSMs (discharged Li_2NH, $MgLi_2(NH)_2$, and Mg_2Si) are indicated. The $T{\cdot}S(H_2(g))$ values are shown by dotted lines for three selected temperatures (25, 60, and 100 °C). The perpendicular box indicates areas where a 'dream H_2 transfer catalyst' should be sought. Solid lines show linear regressions for subsets of five $\{\Delta E_{det}; \Delta E^{\#}_{det}\}$ and five $\{\Delta E_{det}; \Delta E^{\#}_{att}\}$ entries.

sively large 0.91 eV. It thus becomes quite apparent that a new approach is required to decrease the $\Delta E^{\#}_{det}$ and $\Delta E^{\#}_{att}$ values while still ensuring favorable thermodynamics for H_2 detachment. We will describe three possible solutions to this important problem in the subsequent sections.

2.2.4. Dehydrogenation to a Thermodynamically Unstable Product Bends the Rule

Let us now consider the second most stable isomer of the product (Figs. 5 and 6, and Table 4). In both the studied systems ($Ti_4B_4H_8^{[II]}$, $Ti_4N_4H_8^{[II]}$), the ΔE_{det} values are 0.22–0.23 eV larger while the $\Delta E^{\#}_{det}$ values are 0.14–0.22 eV smaller, as compared to the corresponding values for the ($Ti_4B_4H_8^{[I]}$, $Ti_4N_4H_8^{[I]}$) isomers. The respective $\Delta E^{\#}_{att}$ values are also much smaller, by 0.28–0.71 eV. Clearly, the general rule 'lower product stability = small energy barrier' does not hold any longer, and exceptions (in terms of negative deviations of $\Delta E^{\#}_{det}$ and $\Delta E^{\#}_{att}$) can be found.

Obviously, these rule-breaking deviations are crucial for H_2 storage and H_2 transfer catalysts. Consider a HSM that is thermodynamically unstable but kinetically too stable to be dehydrogenated at ambient conditions (say, ΔE_{det} is ca. 0.0 eV, like for some BNH_x compounds, while $\Delta E^{\#}_{det}$ is 1.0 eV). If the dehydrogenation reaction can be directed towards less stable products (for example, where ΔE_{det} is ca. 0.4 eV), along a path which shows a much smaller barrier (for example, 0.5 eV), then the reaction might proceed to the kinetic instead of the thermodynamic product; one might even envisage fully reversible systems of this kind. A similar feature may also be crucial for catalysts; large turnover values may be achievable before the hydrogenated form of a catalyst gets stuck for good in a global energy minimum.

2.2.5. Molecular Analogues of Near-Surface Alloys

The concept of near-surface alloys has recently allowed control over the energy barrier of H_2 attachment reactions at metallic surfaces.[36] We now extend this idea to molecular systems, in order to engineer the values of ΔE_{det}, $\Delta E^{\#}_{det}$, and $\Delta E^{\#}_{att}$. Once again, we use the well-studied $Ti_4C_4H_8$ molecule as the base system for successive perturbations (Fig. 2A).

Figure 7A shows the $Ti_4C_4H_6$ unit of the H_2C complex; the uppermost TiC moiety is the reaction center where H_2 attaches from the gas phase in a complex chemical reaction. Here, the process has been captured at an intermediate stage (dihydrogen complex). An empty (coordinatively unsaturated) TiC edge of the cubic Ti_4C_4 core can be regarded—analogous to extended subsurface alloys—as an isolated TiC ad-unit on the surface of a solid (Fig. 7B). The neighboring $Ti_2C_2H_4$ unit of the molecule corresponds to a surface layer with a TiC stoichiometry (in the molecule, Ti and C are saturated with H atoms; in a solid, they form bonds to the neighboring atoms). The remaining HTiCH unit (at the bottom of Fig. 7B) represents the

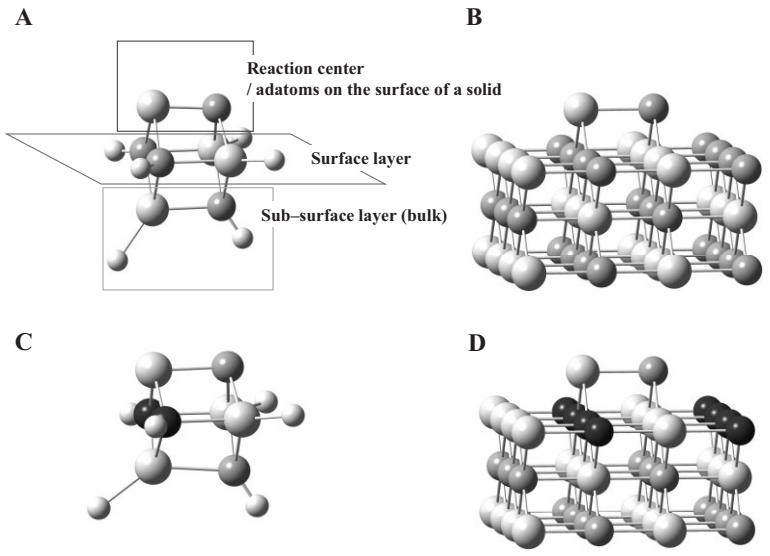

Figure 7. Illustration of the idea of near-surface alloys as applied to molecules. A) The $Ti_4C_4H_6$ molecule; B) an isolated TiC ad-unit attached to the unrelaxed (110) surface of a TiC solid; C) the $Ti_4C_2N_2H_6$ molecule; D) an isolated TiC ad-unit attached to the (110) surface layer of a near-surface alloy. Here, a surface slab with a TiN stoichiometry is deposited on bulk TiC (NaCl structure). The uppermost (coordinatively unsaturated) TiC edge of (A) and (C) is the reaction center (H_2 would be attached here); it corresponds to the exposed TiC ad-unit in (B) and (D). The neighboring $Ti_2C_2H_4$ unit in molecule (A) corresponds to the surface layer of (B) (in the molecule, Ti and C are saturated with H atoms, in (B) they form bonds to the neighbors). The $Ti_2N_2H_4$ unit of molecule (C) corresponds to the TiN surface layer of (D). The remaining HTiCH unit (at the bottom in (A) and (C)) represents a subsurface slab (approximately bulk) with a TiC stoichiometry ((B) and (D)).

subsurface slab of solid TiC. Summarizing, the $Ti_4C_4H_6$ molecule serves as a model for a TiC ad-unit adsorbed on the (110) surface of bulk TiC (which crystallizes in the cubic NaCl structure).

The chemical composition of the i) ad-unit, ii) surface layer, and iii) subsurface layer can of course be varied, thus leading to improvements or deteriorations in the ΔE_{det}, $\Delta E^{\#}_{det}$, and $\Delta E^{\#}_{att}$ values. We could have changed all the components simultaneously and gathered very large set of numerical data, but instead we have opted for a simpler approach. To develop a more detailed understanding, we have chosen to study a narrower set of deliberately perturbed molecules. Therefore, we have retained the $TiCH_2$ composition of the ad-unit and the subsurface layer, and have varied only the surface layer. Such variations may perhaps be realizable experimentally by the epitaxial growth of (MNm) overlayers on the surface of bulk TiC, and by the subsequent attachment of isolated TiC ad-units to the top surface. These variations should indirectly affect the ΔE_{det}, $\Delta E^{\#}_{det}$, and $\Delta E^{\#}_{att}$ values for the process

$$(TiCH_2)(M_2Nm_2H_4)(\mathbf{TiCH_2}) \rightarrow (TiCH_2)(M_2Nm_2H_4)(\mathbf{TiC}) + \mathbf{H_2} \quad (19)$$

and can be simultaneously or separately implemented at the M and Nm sites.

We have tested this idea by introducing several atom-by-atom substitutions to the parent $Ti_4C_4H_8$ system. All these substitutions affect the electron count of the $(MNmH_2)_2$ unit; the electron count varies from 18 for a TiB composition, to 20 for TiC, and 22 for TiN and VC. The TiC → TiB perturbation corresponds to introducing a less electron-rich (more acidic) surface layer to the solid; while in contrast, the TiC → TiN and TiC → VC perturbations result in the TiC ad-unit being attached to a more basic (electron-donating) surface (Fig. 2F). A chemist will naturally expect that the enhanced acidity of the surface layer will allow for stronger binding of the carbide anion and weaker binding of the Ti cation from the TiC ad-unit. Indeed, the optimized geometry of $Ti_4C_2B_2H_6$ (see Sections S6 and S12 in the Supporting Information) is consistent with these predictions.

However, what are the actual results for quantum mechanical calculations of the ΔE_{det}, $\Delta E^{\#}_{det}$, and $\Delta E^{\#}_{att}$ values? It turns out that the substitutions discussed above do not have a very large influence the thermodynamics and kinetics of the H_2 detachment reaction. The range of the ΔE_{det} values is ca. 0.3 eV, while the $\Delta E^{\#}_{det}$ and $\Delta E^{\#}_{att}$ values are spread over ca. 0.1 and ca. 0.2 eV, respectively. The more basic surface layer (TiN) enhances the stability of the $TiCH_2$ ad-unit, whereas the more acidic layer (TiB) tends to diminish it. At this point, molecular analogues of near-surface alloys enjoy limited success; the 'large product stability = large energy barrier' scenario invariably persists.

2.2.6. Interstitial Hydrides Lead the Way

To our delight, as shown in Table 4 and Figure 6, there are two molecules which show desirable thermodynamics and kinetics for H_2 attachment/detachment. These are $Ti_4Si_4H_8$* and its Zr homologue. Both molecules are essentially 'interstitial hydrides', i.e., the hydrogenated reaction center ($MSiH_2$ ad-unit) displays one bridging (three-center) M···H···Si bond and one terminal M–H bond. These molecules also have cubane-like isomers (with one terminal MH and one terminal SiH bond at the $MSiH_2$ ad-unit), discussed above in Section 2.1.1, which are thermodynamically slightly less stable. The heavier Zr derivative has similar properties as the Ti homologue, so we will focus primarily on the latter structure.

The $\Delta E^{\#}_{det}$ and $\Delta E^{\#}_{att}$ values for $Ti_4Si_4H_8$* are, respectively, 0.31 (0.27) eV and 0.00 (0.07) eV (the parenthetical values have not been corrected for the zero-point energies (ZPEs)),[45] vastly different from other similar molecules studied in this contribution. The ΔE_{det} value is 0.49 (0.50) eV. $Ti_4Si_4H_8$* thus shows all the attributes of a 'dream catalyst'. A wish list of properties for such a 'dream catalyst' includes: i) negligible (ca. 0 eV) electronic barrier for the detachment of H_2; ii) as small a barrier as possible for H_2 attachment to its dehydrogenated form, but within the limits of favorable thermodynamics

ADVANCED FUNCTIONAL MATERIALS

(ca. 0.4 eV), and as a consequence of (i) and (ii), an ultrafast kinetics for charging/discharging at virtually neutral thermodynamics; iii) a relatively small $H^+\cdots H^-$ interatomic separation for the hydrogenated form, which would facilitate H_2 transfer from the catalyst to the discharged HSM; and iv) a molecular nature, to ensure easy dispersion in the storage material, as well as catalytic activity at virtually every reaction center.

With its favorable thermodynamic parameters and an $H^+\cdots H^-$ separation of 2.24 Å, $Ti_4Si_4H_8$* shows all the desired features.

The 'interstitial' nature of the Ti–Si and Zr–Si hydrides seems to be the main reason for their unique favorable properties.[46] It has been well established that a majority of covalent and ionic hydrides shows sluggish kinetics for H_2 uptake, while interstitial hydrides (such as those used in metal-hydride batteries) typically allow for fast recharge and discharge at the expense of a low wt % of H stored in these materials. The ease of formation of bridging Ti···H···Si bonds (not observed for analogous $TiCH_x$ systems) reflects the more metallic nature of Si as compared to C, and is also due to the comparable energies of the Ti–H and Si–H bonds. Indeed, the formation of bridging Ti···H···Si bonds has been observed experimentally in $TiSiH_4$.[47]

It thus seems that the successful $Ti_4Si_4H_8$* molecule is essentially a 'golden mean' between covalent and metallic hydrides. A careful study of this system will hopefully allow us to identify the crucial molecular properties which are needed to function as a 'dream catalyst', and allow further expansion of the list of prospective catalytic systems.

2.3. How Does the Most Successful Catalyst Work?

What is the modus operandi of the $Ti_4Si_4H_8$* catalyst candidate? How and why does it differ from other molecules such as $Ti_4C_4H_8$? We will attempt to answer these important questions while unraveling the molecular scale mechanism for H_2 attachment for the best catalyst candidate studied in this report.

2.3.1. Reaction Path for the Dehydrogenation Process

To set the stage, let us first analyze changes in the molecular geometry and atomic polar tensor (APT) charges for various species,[48] along a schematic reaction path for the process,

$$\begin{aligned} Ti_4Si_4H_6 + H_2 \rightarrow Ti_4Si_4H_6\cdots H_2\ (H_2C) \rightarrow TS1 \\ \rightarrow Ti_4Si_4H_8^* \rightarrow TS2 \rightarrow Ti_4Si_4H_8 \end{aligned} \quad (20)$$

where TS1 and TS2 represent two transition states. These changes are illustrated in Figure 8. Let us analyze them from the perspective of the main player in the addition reaction, i.e., the H_2 molecule.

The reaction begins with the (barrierless) attachment of H_2 to an unsaturated Ti site. The H–H bond (0.74 Å in H_2) becomes slightly elongated (0.80 Å), indicating the formation of a classical dihydrogen complex. This is also confirmed by the red-shift of the H–H stretching mode, from a calculated value of 4420 cm^{-1} for free H_2, down to 3458 cm^{-1} for H_2C, and by the appearance of the Ti···(H_2) stretching mode at 701 cm^{-1}. At this stage, the H_2 molecule acts as a weak base, experiencing a small $H^{\delta+}H^{\delta-}$ polarization; however, overall it is forced to share the positive charge residing on the Ti center. Then, at an indiscernible expense of 0.07 eV (electronic barrier, not corrected for ZPE), an electronically flexible molecule reaches the first TS, TS1. Now, the H–H separation increases substantially (to 1.05 Å), but the energy needed to stretch the H–H vibron is largely compensated by the formation of a multicenter Si···H···H···Ti bonding arrangement. A large local electric field originating from the polarized SiTi unit is able to polarize the H_2 molecule ($H^{\delta+}H^{\delta-}$) even more; the APT charges on the H atoms are now –0.28 and +0.32 e. The polarization of H_2 is achieved by the mixing of its σ and σ* orbitals in an asymmetric environment. TS1, like all transition states, cannot be described by just one reasonable Lewis structure. Si and Ti atoms are forced to share one H atom, which is at a nearly equal distance from the two (1.87 and 1.83 Å, respectively). The other H atom is bound to Ti with a bond length of 1.80 Å, and is also still, albeit weakly, bonded to its H partner.

Subsequently, the reaction proceeds from TS1 to the $Ti_4Si_4H_8$* product. This is accompanied by an appreciable energy gain of ca. 0.3 eV. The three-center bonds are destroyed, and the concomitant change in the H–H distance (up to 2.24 Å) clearly suggests that the H atoms are no longer bonded together. In more formal terms, this molecule can be called a 'hydride'.[49] $Ti_4Si_4H_8$* displays an interesting bonding pattern. There is one terminal TiH_{term} bond at 1.72 Å (this H atom is, of course, a negatively charged classical hydride), which shows a regular Ti–H stretching frequency of 1658 cm^{-1}. The second H, bound more strongly to Si (at 1.55 Å), is still engaged in an interaction with the acidic Ti center (at a distance of 1.97 Å). This is reflected in the vibrational spectra: the soft $Si–H_{bridge}$ stretching mode (at 1836 cm^{-1}, can alternatively be viewed as a $Ti\cdots H_{bridge}$ bending mode) appears at twice the frequency of the $Ti–H_{bridge}$ stretching mode (at 902 cm^{-1}, equivalent to $Si–H_{bridge}$ bending). There is almost no charge on this strange 'interstitial' H_{bridge} species. A similar unusual bonding situation comprising both ionic (TiH_{term}) and covalent components ($Si\cdots H_{bridge}\cdots Ti$) also prevails in the $Zr_4Si_4H_8$* analogue.

Let us return to Equation 20; $Ti_4Si_4H_8$* can be further transformed to the cubane-like $Ti_4Si_4H_8$ isomer. In this case and for the Zr analogue, the cubane-like isomer is slightly less stable (by 0.14 eV), but we have still examined this transformation since it may be of importance to other related systems.

The isomerization process is associated with small energy changes, since it is realized by the soft bending of the interstitial H atom around the Si center. Indeed, the molecule climbs only 0.15 eV from $Ti_4Si_4H_8$* to reach the TS, TS2, and then smoothly slides down by a mere 0.01 eV to yield the final product. The interstitial H atom does not encounter large changes in the charge it carries: from –0.02 e for $Ti_4Si_4H_8$*, to –0.06 e in the TS, and finally to –0.09 e for $Ti_4Si_4H_8$. The Si–H bonding is substantially covalent, as seen before for SiH_4. The tetrahedral $Ti_4Si_4H_8$ molecule now shows regular stiff Si–H stretching modes (at 2156–2159 cm^{-1}) and usual Ti–H stretching vibrons

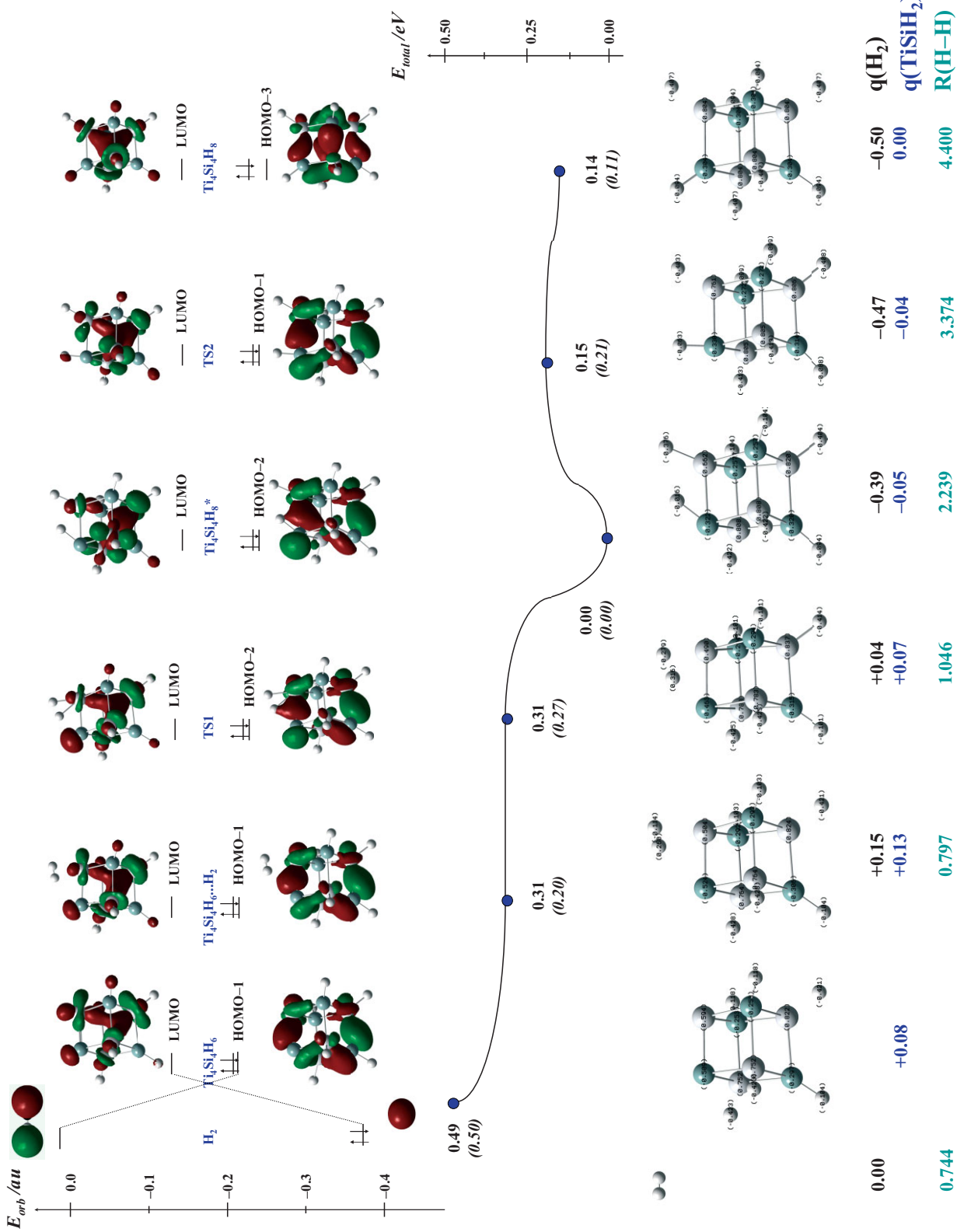

Figure 8. Changes of the total energy, molecular geometry, APT charges on atoms, and chosen MOs for various species involved in the reaction depicted by Equation 20.

ADVANCED FUNCTIONAL MATERIALS

(at 1660–1673 cm^{-1}). The H···H separation is now very large, 4.40 Å, and this is where the H_2 cleavage process (formally a heterolytic cleavage) ends.

Of course, the Ti–Si bond gets elongated during H_2 attachment; the Ti–Si bond length changes from 2.355 Å for $Ti_4Si_4H_6$, to 2.359 Å for $Ti_4Si_4H_6{\cdots}H_2$, 2.388 Å for TS1, and then to 2.505 Å for $Ti_4Si_4H_8$*; upon reaching TS2 it increases again (to 2.601 Å), and then slightly decreases to 2.543 Å for the $Ti_4Si_4H_8$ isomer.

2.3.2. Frontier Orbitals of the Reaction Substrate, Intermediate, Transition States, and Products

It is now worthwhile to look closely at the orbital structures of the reaction substrate, transition states, and products. Naturally, we will concentrate on the MOs in the vicinity of the frontier orbitals for these systems. Changes in the total electron density, electrostatic potential, and other important MOs are shown in Section S10 of the Supporting Information.

The H_2 attachment process described so far preserves the symmetry plane, as determined by the TiSi ad-unit and the H_2 molecule. Since two crucial orbitals of H_2 (σ and σ*) are both symmetric with respect to this plane (i.e., A′), our analysis—in the spirit of the Woodward–Hoffman rules—must take into account the A′ orbitals. A careful examination of the MO structure of $Ti_4Si_4H_6$ (Fig. 8) reveals that the HOMO is A″; fortunately, the LUMO and HOMO − 1 (virtually degenerate with the HOMO) are both A′. The facile heterolytic cleavage of the H–H bond necessarily has to involve these two MOs.

There is a moderate reorganization of the electron density when the H_2C complex is formed. The σ MO of H_2 interacts with the LUMO of $Ti_4Si_4H_6$, and the σ* of H_2 interacts with the HOMO − 1 of $Ti_4Si_4H_6$. However, the former effect is slightly stronger and net charge transfer (0.13 e) takes place from H_2 to $Ti_4Si_4H_6$. Indeed, the σ orbital of H_2 is now found at an energy > 0.1 au lower than in the free molecule; its antibonding counterpart σ* is also stabilized (Supporting Information). However, more substantial changes take place when the reaction progresses via TS1 to $Ti_4Si_4H_8$*, and then via TS2 to $Ti_4Si_4H_8$. The general picture (compare Fig. 8 and Supporting Information) must of course be such that the weak Ti=Si bond (note orbital No. 72 of $Ti_4Si_4H_6$, Supporting Information)[50] and the σ bond of H_2 are progressively substituted by two new σ bonds, TiH and SiH. This is associated with the appearance of σ orbitals for the newly formed Si–H unit (orbitals Nos. 57 and 58 of $Ti_4Si_4H_8$*), as well as for the Ti–H bond (No. 68). Analogous σ orbitals for the $Ti_4Si_4H_8$ isomer are at similar energies. Finally, the interstitial nature of TS1 and $Ti_4Si_4H_8$* (i.e., the presence of multicenter bonds) is clearly seen in the MO picture.

The energy scale is densely packed with many nonbonding and antibonding states of the $Ti_4Si_4H_6$ molecule possessing the correct A′ symmetry, all available for interaction with σ orbitals of H_2. Also, the broad spectrum of bonding MOs of $Ti_4Si_4H_6$ are available for step-by-step mixing with the virtual σ* of H_2. We argue that such flexibility of the frontier orbital manifold is an essential feature for a prospective catalyst, and is absolutely critical to its function. We believe that this feature combined with adequate Ti–Si interatomic separation, and with the sufficiently large spatial extent of frontier orbitals on Ti and Si (which are able to spread to reach the H_2 σ and σ*), ensures low barriers for H_2 attachment and detachment.

A critical question that remains to be answered is how our findings can be useful for designing real hydrogen storage systems.

2.3.3. Practical Implications of the Ease of H_2 Transfer by $Ti_4Si_4H_8$*

The moderate H···H separation (2.24 Å) in $Ti_4Si_4H_8$ provides an exciting opportunity; both the H atoms can now be transferred to the discharged lightweight HSM in a concerted cis manner (Fig. 9), according to Equation 21

$$Ti_4Si_4H_8^* + X^{\delta+}Y^{\delta-} \rightarrow \{\text{active complex}\} \rightarrow Ti_4Si_4H_6 + \textit{cis}\text{-HXYH} \quad (21)$$

where XY represents the discharged, and HXYH the charged proton–hydride HSM.[51] During this process $Ti_4Si_4H_6$ gets reactivated and can be reused.

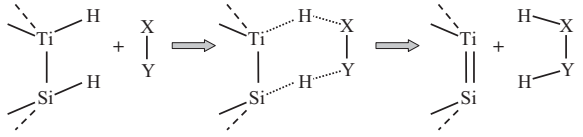

Figure 9. Schematic illustration of H_2 transfer from the hydrogenated form of a catalyst (represented by the Si···H···Ti–H unit) to the discharged HSM (XY). The concerted cis-specific reaction proceeds with reactivation of the dehydrogenated form of the catalyst (Si=Ti) and yields the charged proton–hydride HSM (HXYH).

Ideally, the H_2 affinity of XY should be slightly larger than that of $Ti_4Si_4H_6$ for the reaction shown in Equation 21 to proceed. Analyzing Table 1 we notice four important HSMs with enthalpies of dehydrogenation close to 0.4 eV, namely Mg_2Si (0.38 eV), $LiH/(MgB_2)_{1/2}$ (0.42 eV), $MgLi_2(NH)_2$ (0.46 eV), and Li_2NH (0.47 eV) (listed as the discharged forms). These values are slightly larger than the H_2 affinity of $Ti_4Si_4H_6$ (0.49 eV), but we must remember that our gas-phase calculations at $T = 0$ K provide just a rough approximation, and to some extent are method-dependent. Moreover, it should be possible to precisely tune the thermodynamics and kinetics of the H_2 detachment process on a coordinatively unsaturated Ti=Si ad-unit by making further atom-by-atom substitutions in the adjacent atomic framework of the molecule.[52] Alternatively, one might be able to influence the H_2 affinity of the >Ti=Si< entity by depositing it on various solid surfaces. We now proceed to briefly discuss this latter possibility.

2.3.4. Catalytic Properties of the Surfaces of Various Ti Silicides

A coordinatively unsaturated >Ti=Si< ad-unit could, in principle, appear as a defect on appropriate surfaces (and crystal edges) of solid Ti and Zr silicides. It could also perhaps be deposited (chemisorbed, etched, or grown from the gas phase) on other support materials with varying unit cell dimensions (compare Fig. 7B and Fig. 7C). Under such conditions, the Ti=Si bond length is expected to be controllable within certain limits. Moreover, the thermodynamic stability of the {HTi···H···Si} configuration with respect to dehydrogenation (and also the associated kinetic parameters) may perhaps encompass a sufficiently broad range of values to be further improved in comparison to the parent $Ti_4Si_4H_8$*.

A number of questions remain. Can the surfaces of various Ti silicides (TiSi, $TiSi_2$, etc.), generated by cracking crystallites in high-energy ball-milling processes, serve as catalysts for H_2 transfer? Could these materials be superior to the known Ti–O and Ti–N benchmark systems, or can they at least be as successful at heterolytically splitting H_2 as other catalysts (such as the surfaces of group 6 disulphides (MoS_2, WS_2))? Alternatively, will they be able to substitute much more expensive precious metal catalysts for large-scale hydrogenations?

Will our catalyst candidates be able to resist decomposition in an aggressive proton–hydride hydrogen storage environment? What will be the catalytic turnover and decrease in the T_{dec} value of the HSM? Will the charging kinetics be fast enough to satisfy demands for on-board charging? Can TiSi derivatives work alongside only one specific HSM, or instead can they be versatile? The charging/discharging of a HSM is a very complex process; the function of the catalyst is not only to transfer H_2, but also to promote slow processes of nucleation and growth for grains of the hydrogenation products. Will our catalysts be able to adequately perform this task?

In order to answer these questions, we have now started preliminary theoretical calculations for selected surfaces of Ti silicides. However, one must realize that a complete theoretical exploration of the rich chemistry of even one novel molecular or solid catalyst candidate is extremely difficult, consuming of resources, and certainly beyond the scope of one paper. We believe that answers may be available—much earlier and with more reliability—from experiments. Extensive research is needed to achieve breakthroughs that will bring emerging proton–hydride hydrogen storage systems even closer to practical reversibility and low-temperature discharge, so as to finally realize the dream of the 'H_2 economy'.

3. Conclusions

In this contribution we have assembled for the first time information on the thermodynamics and thermal decomposition of emerging (since 2002) proton–hydride solid HSMs. It turns out that there are four lightweight chemical reservoirs (the discharged forms being Li_2NH, $Li_2Mg(NH)_2$, Mg_2Si, and LiH/MgB_2) that show favorable thermodynamics for H_2 attachment. However, these materials suffer from sluggish kinetics for the charging/discharging processes and exhibit high T_{dec} values. Theoretically, these shortcomings, critical for on-board use, might be improved by the use of proper catalysts.

We have thus concentrated on the first-principles design of novel catalysts for the heterolytic splitting of H_2. We have studied the thermodynamics of H_2 detachment and the associated energy barriers for molecular catalyst candidates with a formula of $M_4Nm_4H_8$ (M = V, Ti, Zr, Hf, Nm = Si, C, B, N). These complex molecules can be obtained from the previously studied $Ti_4C_4H_8$ systems[23] by deliberate isoelectronic substitutions, step-by-step variation of the valence electron count, and by transferring the idea of near-surface alloys from extended solids to molecular systems. Systematic perturbations of the parent $Ti_4C_4H_8$ molecule has helped us to prove that the rule coupling the kinetics of a process with its thermodynamics[1] can indeed be bent.

Our results show that it may be possible to simultaneously combine neutral thermodynamics for H_2 addition with fast kinetics. The $Ti_4Si_4H_6$ molecule (with a coordinatively unsaturated >Ti=Si< unit at one edge of a Ti_4Si_4 cube) exhibits particularly favorable thermodynamics and has an unusually small electronic barrier for H_2 attachment (>0.07 eV); the product of this reaction ($Ti_4Si_4H_8$*, with one interstitial H atom) also exhibits a very small barrier for H_2 detachment (>0.27 eV) and we have studied this process in greater detail. This has enabled us to formulate several important prerequisites for facile H_2 transfer. The remedy for kinetic obstacles lies in the unique electronic structure and bond length of the Ti=Si unit, which is able to form multicenter bonds with two interstitial H atoms in the TS.

The molecular materials studied in silico here could indeed be precursors for genuine catalysts for the heterolytic splitting of H_2. However, as our knowledge of these systems is still fragmentary and we have just studied a narrow set of molecules here, the properties of these and related systems need to be verified by experimental efforts. Our results suggest some promising directions for experimental research: a) $Ti_4Si_4H_6$ and its derivatives (for example, $[(Cp)_3Ti_3][Si_3Cl_3][TiSi]$) may be possible to synthesize in noble gas matrices, and can subsequently be used for H_2 attachment; b) chemical substitutions in the atomic framework of $Ti_4Si_4H_6$ may lead to organometallic compounds that are carefully crafted to function as catalysts; c) >Ti=Si< ad-units can perhaps be chemisorbed on various support materials (such as the (110) surface of HfC) in order to influence the thermodynamics and kinetics of H_2 attachment in a desired direction; and d) defects resembling >Ti=Si< ad-units can perhaps be generated on surfaces and edges of solid Ti silicides (for example, by ball-milling) and tested for their catalytic activity.

4. Experimental

Computational Methods: Our DFT computations were performed with the B3LYP correlation-exchange function. We used Pople's basis set (6-311++G** for C, Si, H, B, and N, and the largest set available, 6-31G**, for Ti and V). The Stuttgart–Dresden (SDD) pseudopotentials [53] were applied for Zr and Hf, followed by a standard double zeta ba-

sis set. These effective core potentials, parameterized consistently for all atoms up to At, largely account for relativistic effects, and have proven to be very successful in reproducing the experimental properties of the hydride/methylidene complexes of Zr and Hf [54].

Test calculations for $Ti_4C_4H_8$ showed that the SDD results were essentially identical to those with Pople's basis set (6-31G**) for a transition metal atom, and were also similar to results obtained using the Los Alamos LANL2DZ pseudopotential (see Secs. S1 and S2 in Supporting Information) [55]. The differences between the SDD and 6-31G** results were particularly small: 0.001 Å for the Ti–C and Ti–H bond lengths, a minor deviation of +0.04 e in the value of APT charges on atoms, no more than 0.001 au (< 0.003 eV) discrepancy for the energy of the frontier orbitals, and negligible differences in the Mulliken electronegativity and Pearson hardness of the molecule. This agreement of the essential molecular features as computed by two different methods gave us confidence in the SDD results for molecules containing Zr and Hf (the complete 6-31G** basis set was not available for these heavy elements). The SDD results for enthalpies of H_2 detachment also differed only negligibly from the 6-31G** ones. For example, the test SDD calculation gave +1.01 eV (the non-zero-point vibrational energy (non-ZPVE) corrected H_2 detachment enthalpy for $Ti_4C_4H_8$), whereas the 6-31G** (Ti) set gave +1.02 eV.

We want to stress that we may not have always found an absolute minimum on the complex potential energy surface for a system with 4 M, 4 Nm, and 8 H nuclei. However, the 'cubane-like' and 'interstitial hydride' minima are very important for our results here, and may serve as cluster models for H_2 chemisorbed in two different ways on MNm adatoms attached to the (110) surface of corresponding MNm solids. This can be of great value in practice, since the computational effort is much smaller for molecular calculations than for ab initio treatments of periodic systems with large unit cells (an accurate model for 'non-interacting defects'). We treat the calculations for molecular models as a prelude to more computationally exhausting studies of related extended systems [56].

All the minima were tested for harmonic frequencies, and did not yield any imaginary values. One imaginary value was seen for the TSs, as listed in the Supporting Information. The reaction energies (calculated at $T = 0$ K) were corrected for the ZPE; these corrections were usually small (up to 0.15 eV) and usually promoted substrates for H_2 detachment reactions due to the large ZPE of the H–H oscillator. Typically, our molecules have an even number of valence electrons and thus we studied only the singlet states. However, for several promising systems (such as for $Zr_4Si_4H_6$, which, formally might contain a Zr(III) d^1/Si(III) $(s,p)^1$ or a high-spin Zr(II) d^2/Si(II) group), we also considered triplet states. It turns out that the singlet state is favored (the lowest-lying triplet state is 0.54 eV above the ground state, i.e., 0.52 eV after ZPVE correction, for $Zr_4Si_4H_6$).

The correct assessment of reaction enthalpy at 298 K requires knowledge of the $\Delta[pdV]$ and $\Delta[C_p dT]$ terms, which are usually small in comparison to the ZPVE-corrected electronic energy changes. As shown by calculations for various hydride materials, the reaction enthalpy typically differs only very little from the ZPVE-corrected reaction energy [57] because of the cancellation of these additional terms for all substrates and products. Therefore, in this work we have interchangeably used the expressions 'reaction energy' and 'reaction enthalpy'.

Received: December 12, 2005
Final version: April 10, 2006
Published online: September 15, 2006

Note added in proof: When this paper was in proof, an interesting report has appeared on the possibility of storing 3 wt % H_2 in sodium oxide.[58]

[1] W. Grochala, P. P. Edwards, *Chem. Rev.* **2004**, *104*, 1283.

[2] Various Ti, V, Nb, Fe, and SiO_2-based catalysts are known to accelerate H_2 uptake and H_2 evolution from HSMs. In addition, novel binuclear Ni^{1+}-based catalysts have recently been suggested by theory, W. Grochala, *Chem. Phys. Phys. Chem.* **2006**, *8*, 1340.

[3] a) P. Chen, Z. T. Xiong, J. Z. Luo, J. Y. Lin, K. L. Tan, *Nature* **2002**, *420*, 302. Note that an interesting family of nitride–hydrides (mixed-anion compounds) is known, including its lightweight representative, Li_4NH. b) R. Marx, *Z. Anorg. Allg. Chem.* **1997**, *623*, 1912. It has been observed that Li_4NH easily reacts with H_2, forming Li_2NH and 2 LiH (4.5 wt % H). The dehydrogenation reaction has not been studied, but we expect that it would be difficult to recover the initial ternary substrate.

[4] Y. Nakamori, G. Kitahara, S. Orimo, *J. Power Sources* **2004**, *138*, 309.

[5] Y. Nakamori, S. Orimo, *Mater. Sci. Eng. B* **2004**, *108*, 48.

[6] a) Y. Nakamori, G. Kitahara, K. Miwa, S. Towata, S. Orimo, *Appl. Phys. A—Mater. Sci. Process.* **2005**, *80*, 1. b) A recent theoretical paper predicts favorable reaction thermodynamics for the dehydration reaction of $(LiNH_2 + MgH_2)$, which leads to the formation of a LiMgN phase: S. V. Alapati, J. K. Johnson, D. S. Sholl, *J. Phys. Chem. B*, **2006**, *110*, 8769.

[7] a) T. Ichikawa, N. Hanada, S. Isobe, H. Leng, H. Fujii, *Mater. Trans.* **2005**, *46*, 1. b) H. Leng, T. Ichikawa, S. Hino, T. Nakagawa, H. Fujii, *J. Phys. Chem. B* **2005**, *109*, 10 744.

[8] a) M. Aoki, K. Miwa, T. Noritake, G. Kitahara, Y. Nakamori, S. Orimo, S. Towata, *Appl. Phys. A—Mater. Sci. Process.* **2005**, *80*, 1409. b) F. E. Pinkerton, G. P. Meisner, M. S. Meyer, M. P. Balogh, M. D. Kundrat, *J. Phys. Chem. B* **2005**, *109*, 6. The crystal structure of another important HSM, $Li_4(BH_4)(NH_2)_2$, has recently been determined by three groups independently: c) Y. E. Filinchuk, K. Yvon, G. P. Meisner, F. E. Pinkerton, M. P. Balogh, *Inorg. Chem.* **2006**, *45*, 1433. d) T. Noritake, M. Aoki, S. Towata, A. Ninomiya, Y. Nakamori, S. Orimo, *Appl. Phys. A—Mater. Sci. Process.* **2006**, *83*, 277. e) P. A. Chater, W. I. F. David, S. R. Johnson, P. P. Edwards, P. A. Anderson, *Chem. Commun.* **2006**, 2439. It turns out that the maximum H_2 storage capacity is achieved for the $(LiNH_2 + 1/3\,LiBH_4)$ compound: f) G. P. Meisner, M. L. Scullin, M. P. Balogh, F. E. Pinkerton, M. S. Meyer, *J. Phys. Chem. B* **2006**, *110*, 4186.

[9] a) J. Lu, Z. Fang, *J. Phys. Chem. B* **2005**, *109*, 20 830. b) Y. Nakamori, A. Ninomiya, G. Kitahara, M. Aoki, T. Noritake, K. Miwa, Y. Kojima, S. Orimo, *J. Power Sources* **2006**, *155*, 447. The authors observe a very small H storage capacity (4.1 wt %) for the $LiAlH_4 + 2\,LiNH_2$ mixture (ball-milled for 1 h), as compared to the theoretical value (9.5 wt %). Surprisingly, the H_2 release is endothermic despite the rather low T_{dec} (100 °C as determined by thermal desorption spectroscopy, or 150 °C as determined by thermogravimetric analysis). Both observations make us believe that a large amount of H_2 is released during ball-milling, and that the authors are in fact dealing with an in situ-generated 2/3 Al/1/3 Li_3AlH_6/2 $LiNH_2$ (or similar) mixture.

[10] Mixtures of $LiNH_2$ with 1/2 MgH_2 transform into 1/2 $Mg(NH_2)_2$ + LiH upon cycling: a) W. Luo, E. Ronnebro, *J. Alloys. Compd.* **2005**, *404*, 392. Compare with b) H. Y. Leng, T. Ichikawa, S. Isobe, S. Hino, N. Hanada, H. Fujii, *J. Alloys. Compd.* **2005**, *404*, 443.

[11] a) C. C. Tang, Y. Bando, X. X. Ding, S. R. Qi, D. Golberg, *J. Am. Chem. Soc.* **2002**, *124*, 14 550. b) X. Chen, X. P. Gao, H. Zhang, Z. Zhou, W. K. Hu, G. L. Pang, H. Y. Zhu, T. Y. Yan, D. Y. Song, *J. Phys. Chem. B* **2005**, *109*, 11 525. Here, ΔH^0 is expected to be positive, since the complete decomposition of hydrogenated BN nanotubes only occurs at temperatures exceeding 300 °C.

[12] a) J. Baumann, E. Baitalow, G. Wolf, *Thermochim. Acta* **2005**, *430*, 9. b) E. Baitalow, J. Baumann, G. Wolf, K. Jaenicke-Rößler, G. Leitner, *Thermochim. Acta* **2002**, *391*, 159. c) G. Wolf, J. Baumann, F. Baitalow, F. P. Hoffmann, *Thermochim. Acta* **2000**, *343*, 19.

[13] A. Gutowska, L. Y. Li, Y. S. Shin, C. M. M. Wang, X. H. S. Li, J. C. Linehan, R. S. Smith, B. D. Kay, B. Schmid, W. Shaw, M. Gutowski, T. Autrey, *Angew. Chem. Int. Ed.* **2005**, *44*, 3578.

[14] a) T. Ichikawa, H. Fujii, S. Isobe, K. Nabeta, *Appl. Phys. Lett.* **2005**, *86*, 241 914. b) T. Ichikawa, S. Isobe, H. Fujii, *Mater. Trans.* **2005**, *46*, 1757.

[15] All thermodynamic data were taken from the National Institute of Standards and Technology (NIST) chemistry database: http://www.nist.gov.

[16] J. J. Vajo, S. L. Skeith, F. Mertens, S. W. Jorgensen, *J. Alloys Compd.* **2005**, *390*, 55.

[17] a) The Millenium Cell Company 'Hydrogen on Demand' technology relies on this reaction, and a broad list of associated heterogeneous transition metal catalysts are now available. This process may be reversed chemically, for example, by the reaction of $2\,MgH_2$ with $NaBO_2$. b) For an analogous process using a Li derivative, see Y. Kojima, Y. Kawai, M. Kimbara, H. Nakanishi, S. Matsumoto, *Int. J. Hydrogen Energy* **2004**, *29*, 1213.

[18] J. J. Vajo, F. Mertens, C. C. Alm, R. C. Bowman, B. Fultz, *J. Phys. Chem. B* **2004**, *108*, 13 977.

[19] a) J. J. Vajo, S. L. Skeith, F. Mertens, *J. Phys. Chem. B* **2005**, *109*, 3719. b) S. R. Johnson, P. A. Anderson, P. P. Edwards, I. Gameson, J. W. Prendergast, M. Al-Mamouri, D. Book, I. R. Harris, J. D. Speight, A. Walton, *Chem. Commun.* **2005**, 2823. c) One can also imagine a process leading from $M(BH_4)_2$ directly to MgB_2; recharging with H_2 is expected to be slow.

[20] Note that the entropy term for gaseous H_2 is about 0.40 eV at 298 K; thus, the enthalpy of H_2 release being +0.40 eV guarantees that $\Delta G^0 \approx 0$.

[21] As one of the referees has correctly reminded us, our rule does not apply to hydride HSMs, such as alanates, borohydrides, and simple hydrides.

[22] D. Chandra, J. J. Reilly, R. Chellappa, *JOM* **2006**, *58*, 26.

[23] Note even an ideal H_2 transfer catalyst cannot guarantee low T_{dec} values for very stable H_2 storage systems.

[24] C. R. S. M. Hampton, I. R. Butler, W. R. Cullen, B. R. James, J. P. Charland, J. W. Simpson, *Inorg. Chem.* **1992**, *31*, 5509.

[25] C. J. Curtis, A. Miedaner, W. W. Ellis, D. L. DuBois, *J. Am. Chem. Soc.* **2002**, *124*, 1918.

[26] M. S. Chinn, D. M. Heinekey, N. G. Payne, C. D. Sofield, *Organometallics* **1989**, *8*, 1824.

[27] a) J. C. Lee, E. Peris, A. L. Rheingold, R. H. Crabtree, *J. Am. Chem. Soc.* **1994**, *116*, 11 014. b) A. J. Lough, S. Park, R. Ramachandran, R. H. Morris, *J. Am. Chem. Soc.* **1994**, *116*, 8356. c) R. H. Morris, *Can. J. Chem.* **1996**, *74*, 1907.

[28] D. Sellmann, G. H. Rackelmann, F. W. Heinemann, *Chem. Eur. J.* **1997**, *3*, 2071.

[29] Z. K. Sweeney, J. L. Polse, R. A. Andersen, R. G. Bergman, M. G. Kubinec, *J. Am. Chem. Soc.* **1997**, *119*, 4543.

[30] R. C. Linck, R. J. Pafford, T. B. Rauchfuss, *J. Am. Chem. Soc.* **2001**, *123*, 8856.

[31] A. Lenco, M. J. Calhorda, J. Reinhold, F. Reineri, C. Bianchini, M. Peruzzini, F. Vizza, C. Mealli, *J. Am. Chem. Soc.* **2004**, *126*, 11 954.

[32] Y. Ohki, N. Matsuura, T. Marumoto, H. Kawaguchi, K. Tatsumi, *J. Am. Chem. Soc.* **2003**, *125*, 7978.

[33] a) I. N. Gogotov, N. A. Zorin, L. T. Serebriakova, *Int. J. Hydrogen Energy* **1991**, *16*, 393. b) M. Pavlov, P. E. M. Siegbahn, M. R. A. Blomberg, R. H. Crabtree, *J. Am. Chem. Soc.* **1998**, *120*, 548.

[34] H. Kato, H. Seino, Y. Mizobe, M. Hidai, *J. Chem. Soc., Dalton Trans.* **2002**, 1494.

[35] W. Grochala, *Chem. Commun.* **2005**, 2330.

[36] B. Bogdanovic, M. Schwickardi, *J. Alloys Compd.* **1997**, *253*, 1.

[37] J. Greeley, M. Mavrikakis, *Nat. Mater.* **2004**, *3*, 810.

[38] W. Grochala, *Pol. J. Chem.* **2005**, *79*, 1087.

[39] The discussed $M_4Nm_4H_8$ molecules may also be useful for the low-temperature chemical vapor deposition of transition metal carbide coatings and novel hypothetical polymorphs of transition metal silicides, such as cubic TiSi. Some of these compounds have unusual properties, for example, the melting temperature of HfC is as high as 3890–3928 °C, comparable to the sublimation temperature of graphite at 1 atm (3915–4020 °C). HfC is also the most refractory material known to man. For a compendium about this subject see H. O. Pierson, *Handbook of Refractory Carbides and Nitrides, and Carbides of Group IV*, Noyes, Park Ridge, NJ **1996**.

[40] Since tetravalent V is much more oxidizing than tetravalent Ti (the standard redox potential of the V^{4+}/V^{3+} pair is +1.00 V, while that of the Ti^{4+}/Ti^{3+} pair is +0.10 V), it is reasonable to expect that the M–H bonds will always be longer and weaker for V than for Ti, which is in agreement with the general picture of M–H bonding [1].

[41] The agostic interaction of the H_B hydrogen with a neighboring Ti atom (Supporting Information) is the most important difference between $Ti_4(B_2N_2)H_8$ and $Ti_4C_4H_8$.

[42] It would be interesting to determine if $Ti_4B_2N_2H_8$ can serve as a precursor for the chemical vapor deposition of $Ti(B_{0.5}N_{0.5})$ solid, an isoelectronic analogue of technologically important titanium carbide.

[43] Notably, a similar monotonic relationship has been also noted for the calculated bond length of the H–B bridging bond (contained in a metal–H–B entity) plotted versus the same thermodynamic parameter. W. Grochala, P. P. Edwards, *J. Alloys Compd.* **2005**, *404–406*, 31.

[44] a) G. S. Hammond, *J. Am. Chem. Soc.* **1955**, *77*, 334. b) D. J. Wales, *Science* **2001**, *293*, 2067.

[45] a) DFT tends to underestimate the electronic barriers, the real $\Delta E^{\#}_{det}$ and $\Delta E^{\#}_{att}$ values may be 50 % larger then the calculated values. b) A negligible barrier for the attachment of H_2 to the TiSi ad-unit, resulting in the formation of {H–Ti···H···Si}, certainly promotes this process kinetically, despite other possible scenarios for hydrogenation, such as those leading to {Ti···H···Si–H}, {H–Ti–Si–H}, {H_2Ti–Si}, or {Ti–SiH_2}.

[46] Compare also the ΔE_{det}, $\Delta E^{\#}_{det}$, and $\Delta E^{\#}_{att}$ values for isoelectronic $Ti_4C_2N_2H_8$ and $Ti_2V_2C_4H_8$* species. All the values are reduced by 0.2–0.3 eV for the V compound; note that $Ti_2V_2C_4H_8$* is an interstitial hydride, while $Ti_4C_2N_2H_8$ is not.

[47] A. Bihlmeier, T. M. Greene, H.-J. Himmel, *Organometallics* **2004**, *23*, 2350. An impressive variety of $TiSiH_4$ isomers have been detected, including those with one, two, or three bridging H atoms.

[48] J. Cioslowski, *J. Am. Chem. Soc.* **1989**, *111*, 8333.

[49] G. J. Kubas, *Metal Dihydrogen and σ Bond Complexes: Structure, Theory and Reactivity*, Kluwer/Plenum, New York **2001**.

[50] The electronic structure of the Ti=Si unit bound by additional chemical bonds is of course very different from that of the isolated ^{5}TiSi molecule. M. Tomonari, K. Tanaka, *Theor. Chem. Acc.* **2001**, *106*, 188.

[51] The details of the mechanism of H_2 release from such storage materials is not known, but it is usually presumed to be initiated by proton–hydride coupling. Here, the proton and hydride anion must first form 'unconventional', i.e., 'dihydrogen' hydrogen bonds: a) R. Custelcean, J. E. Jackson, *Chem. Rev.* **2001**, *101*, 1963. b) N. V. Belkova, E. S. Shubina, L. M. Epstein, *Acc. Chem. Res.* **2005**, *38*, 624.

[52] Our preliminary calculations show that the ΔE_{det} of $Ti_4Si_4H_8$* (0.49 eV) can indeed be tuned in molecular analogues of near-surface alloys, as exemplified by values of 0.60 eV for $(TiSiH_2)(Hf_2C_2H_4)(TiSiH_2)$* and 0.43 eV for $(TiSiH_2)(Ti_2N_2)(TiSiH_2)$*.

[53] D. Andrae, U. Haeussermann, M. Dolg, H. Stoll, H. Preuss, *Theor. Chim. Acta* **1990**, *77*, 123.

[54] a) H. G. Cho, X. F. Wang, L. Andrews, *J. Am. Chem. Soc.* **2005**, *127*, 465. b) H. G. Cho, L. Andrews, *J. Phys. Chem. A* **2004**, *108*, 10 441.

[55] H. G. Cho, L. Andrews, *J. Phys. Chem. A* **2004**, *108*, 3965.

[56] Ł. Maj, W. Grochala, unpublished.

[57] a) W. Wolf, J. Sticht, A. Mavromaras, B. Leblanc, P. Saxe, E. Wimmer, *Mater. Sci.—Pol.* **2005**, *23*, 365. b) E. Wimmer, *Mater. Sci.—Pol.* **2005**, *23*, 325.

[58] Q. Xu, R. T. Tang, T. Kiyobayashi, N. Kuriyama, T. Kobayashi, *J. Power Sources* **2006**, *155*, 167.